Doctoral dissertation

Studies on multielectron-transfer mechanism in heterogeneous photocatalytic oxygen evolution

光触媒酸素生成反応における多電子移動機構に関する研究

Division of Environmental Materials Science
Graduate School of Environmental Science
Hokkaido University

Shugo Takeuchi

Table of contents

Chapter 1

General Introduction

1-1 Heterogeneous Photocatalysis

"Heterogeneous photocatalysis" is defined as photochemical reactions occurring at heterogeneous interphase of solid-liquid or solid-gas phases by photoabsorption of the solid material as a "photocatalyst", while "homogeneous photocatalysis" is driven by a photoabsorbing molecules or metal complexes, as a "photocatalyst", dissolved in a solvent containing reaction substrates. In this thesis, the term "photocatalyst" is used only for a solid photocatalyst used in heterogeneous photocatalysis. Even though a word "catalysis" is included in the term "photocatalysis", the concepts of "photocatalysis" and "catalysis" are different with each other and, in this sense, photocatalysts cannot be catalysts in their definition. Such difference arises from the principle of photocatalysis. While catalytic reactions proceed at "active sites" on a catalyst enabling reduction of activation energy of a given negative Gibbs energy-change reaction, photocatalytic reactions can drive both negative (energy releasing) and positive (energy storing) Gibbs energy-change reactions through redox processes induced by photoirradiation.

Figure 1-1 shows an energy diagram, so-called "band-structure model", of semiconducting materials as a representative photocatalyst. Although "photocatalysts" are not limited only to semiconducting materials, solid materials which are not categorized to semiconductors have similar electronic structures and behave similarly [Ohtani 2014]. The band-structure model consists of electron-filled valence band (VB), electron-empty conduction band (CB) and forbidden band (or "bandgap") dividing CB and VB. When light of energy higher than the bandgap is irradiated, electrons in VB are excited by absorbing the energy of light into CB leaving positive holes, virtual particles possessing positive charge. The thus liberated photoexcited electrons and positive holes can migrate to the surface of photocatalysts and react with substrates adsorbed on the surface to result in their reduction and oxidation, respectively, and otherwise undergo recombination to give no net chemical reaction. Thus, photocatalytic reactions are initiated by those redox reaction with photoexcited electrons and positive holes.

It has been widely accepted in the field of photocatalysis that the required conditions for photocatalytic reactions, from the standpoint of thermodynamics, are (i) CB-bottom energy, i.e., reducing ability of photoexcited electrons, is higher (more cathodic) than the

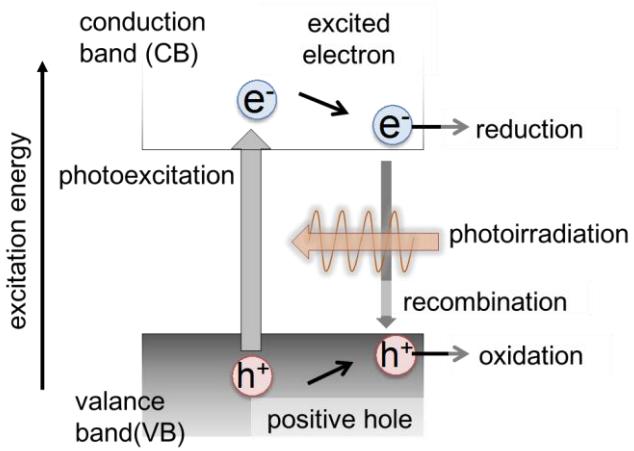

Fig.1-1 Principle of photocatalysis based on a band-structure model

standard electrode potential (SEP; The definition is discussed in **Section 1-8**.) of a substrate to be reduced and (ii) VB-top energy, i.e., oxidizing ability of positive holes, is lower (more anodic) than the SEP of a substrate to be oxidized. Therefore, as described in the previous section, energy-storing reactions with positive Gibbs-energy change may occur in photocatalysis. Such a characteristic is not limited to heterogeneous photocatalysis; the required conditions for homogeneous photocatalysis are the energies of LUMO (lowest unoccupied molecular orbital) and HOMO (highest occupied molecular orbital) of a given molecular/metal-complex photocatalyst are higher and lower than the SEPs of substrate to be reduced and oxidized, respectively. In this sense, intrinsic principles of heterogeneous and homogeneous photocatalyses are the same.

1-2 Titanium Oxide(IV) Photocatalyst

Titanium(IV) oxide (titania) is the most widely used photocatalyst owing to its high abundance (of the element of titanium), relative cheapness (due to high industrial demands as a pigment), non toxicity (in a practical sense), high photostability and at least appreciable photocatalytic activity. Although titania absorbs only ultraviolet (UV) light and visible-light cannot be utilized in titania photocatalysis, the color of base materials coated or deposited with titania is kept unchanged since titania does not absorb visible light and this is also an advantage of a titania photocatalyst. Therefore, titania has been used in fundamental studies and practical applications of heterogeneous photocatalysis, and even when non-titania photocatalysts are used, those performance has been (and will be) compared with that of titania. It has been reported that the bandgap of titania is 3.0–3.2 eV, depending on its crystal polymorphs, and CB-bottom and VB-top positions are suitable for

reduction and oxidation, respectively, of a wide range of substrates, e.g., water and carbon dioxide [Kavan 1996].

1-3 Effect of Crystalline Structure of Titania Photocatalysts

Since the aforementioned band structure is defined only for crystalline solids and the band positions depend only on crystalline form, photocatalytic activities, the most significant performance, of photocatalysts in correlation to their crystalline forms has often been discussed [Mills 1982/Roger 1990/Fujihara 1998/Fujihara 2000/Ozawa 2007/Paola 2007/Valdes 2007/Yamakata 2015/Li 2015]. It has generally been recognized that among three natural polymorphs (anatase, rutile and brookite) anatase, the most industrially produced crystalline form of titania, shows higher photocatalytic activities for decomposition of organic compounds under aerobic conditions than rutile, the most naturally abundant form of titania [Mills 1982/Paola 2007/Valdes 2007], while, for the oxidation of water into oxygen under deaerated conditions, rutile and anatase show high and negligible photocatalytic activities, respectively [Mills 1982/Fujihara 2000]. Such difference in photocatalytic activities has been discussed predominantly from the standpoint of thermodynamics using the band-structure model, which seems rather strange because photocatalytic activities are evaluated with the rate of photocatalytic reaction and therefore photocatalytic activities should be discussed from the standpoint of kinetics, not thermodynamics. The discussion claimed that the organics decomposition is driven by anatase, the CB-bottom position of which is reported a little higher (more cathodic) than the SEP for one-electron reduction of oxygen {$O_2 + e^- = O_2^{\cdot -}$; –0.28 V vs SHE (standard hydrogen electrode) [Bard 1985]} with higher efficiency than rutile possessing the lower CB-bottom energy possibly to reduce with two electron-transfer process ($O_2 + 2e^- = H_2O_2$; +0.70 V vs SHE [Bard 1985]).

An example of the other discussion on the effect of crystalline structure on the photocatalytic activity not related to the band-structure model was based on the difference in reaction intermediates; difference in intermediate radical species possible liberated on anatase and rutile surfaces caused the difference in photocatalytic activities for organics decomposition [Li 2015/Valdes 2007]. Lifetime of charge carriers, photoexcited electrons and positive holes, has been also discussed in relation to photocatalytic activities; longer lifetime of charge carrier in rutile, which is due to electron trapping by its lattice defects, was elucidated on the basis of observation that higher efficiency of rutile for oxygen evolution than anatase and decay time course of transient absorption [Li 2015/Yamakata 2015]. In another report, band bending in a rutile photocatalyst particle in contact with electrolyte solutions was suggested to be an important factor for photocatalytic oxygen

evolution and the lower anatase photocatalytic activity was attributable to the negligible band bending [Fujihara 1998/Fujihara 2000].

The above-mentioned discussion seems consistent with the practical experimental results and it is impossible to be excluded, but it seems that no attempts have been made for kinetic analysis which includes the first step of photocatalysis, photoabsorption, of heterogeneous photocatalysis.

1-4 Effect of Particle Size of Titania Photocatalysts

It is believed in the field of photocatalysis that particle size of photocatalysts is the most significant decisive factor of photocatalytic activities and almost all the discussion was made considering specific surface area, which is closely related to particle size, of photocatalysts. As a general de-facto understanding, the smaller the particle size is, i.e., the higher the specific surface area is, the higher becomes the photocatalytic activity (and vise versa) in photocatalytic organics decomposition due to the higher surface concentration of adsorbed reaction substrates [Prieto 2009/Ohtani 2010]. Since anatase crystallites were converted into rutile crystallites upon heating and calcination induce the enlargement of crystallites and therefore the reduction of specific surface area, commercial and laboratory-made anatase samples tend to be of smaller particle size and higher specific surface area and to show relatively higher photocatalytic activity for organics decomposition than rutile samples. On the contrary, reversed tendency was often observed in photocatalytic oxygen evolution reaction, i.e., water oxidation; the larger the (secondary) particle size is, the higher becomes the photocatalytic activity, and as described above rutile particles seemed favorable [Prieto 2009, Ohtani 2010]. In the discussion on the influence of calcination on the activities of rutile titania and tungsten(VI) oxide (tungstena) for photocatalytic oxygen evolution, the rutile activity was increased with the calcination temperature-dependent particle size [Maeda 2014], presumably due to higher crystallinity and density of electron-donating oxygen vacancy, and the activity of tungstena was improved by enlargement of particle size [Hong 2009/Amano 2013], presumably due to decrease in surface recombination processes [Amano 2013] or in crystallinity and surface charge layer [Hong 2009].

In those studies correlation of photocatalytic activity with particle size (specific surface area) was discussed from the standpoint of kinetics, not thermodynamics; reaction rate of steps, e.g., oxidation of surface-adsorbed substrates with positive holes and/or charge-carrier migration and recombination of charge carriers, may be regulated by the particle size (specific surface area)-related properties. However, effect of particle size (specific surface area) on the initial photoabsorption step was not taken into consideration. Moreover, no

discussion was made taking the number of photoexcited electrons and positive holes in a photocatalyst particle into consideration even though the latter photocatalytic oxidation of water requires four-electron (positive hole) transfer in formal.

1-5 Effect of Kinds of Electron Acceptors for Oxygen Evolution

The oxygen evolution from water, a representative multielectron-transfer process, is a half-cell (oxidation) reaction and thereby any counter half-cell reduction reaction can be combined to the oxygen evolution. In the photolysis of water into oxygen and hydrogen, as discussed later, the counter half-cell reduction reaction is hydrogen evolution from water. It is well known that the photocatalytic oxygen evolution from water is enhanced when appropriate electron acceptors to capture photoexcited electrons of a photocatalyst are added in the photocatalytic reaction systems (In the photocatalytic organics decomposition, oxygen works as the electron acceptor.).

Several kinds of electron acceptors have been used in the studies on photocatalytic oxygen evolution, e.g., silver(I) ion (Ag^{+}) [Nishimoto 1983], iron(III) ion (Fe^{3+}) [Mills 1982/Ohno 1997], iodate ion (IO_3^{-}) [Sayama 2001] and persulfate ion ($S_2O_8^{2-}$) [Hong 2008, Puntriero 2010]. For example, photocatalytic activities of titania and tungstena for oxygen evolution was studied using Fe^{3+} and cerium (IV) ion (Ce^{4+}) as an electron acceptor [Bamwenda 2001] and concluded that charges of both photocatalyst surface and electron-acceptor ions might govern the forward (photocatalyst-to-acceptor) and backward (acceptor-to-photocatalyst) electron-transfer processes. The rate of backward electron transfer was also studied using titania and Fe^{3+} as photocatalyst and electron acceptor, respectively [Fujihara 1998].

Therefore, for the studies on oxygen evolution, the rate (or photocatalytic activity) might be influenced by the kinds of electron acceptors added in the photocatalytic reaction systems. Another point worth noting is the number of electrons transferred to those electron acceptors; it is generally presumed that Ag^{+} and Fe^{3+} accept single electron, while IO_3^{-} accepts multiple electrons. This may also affect the overall rate of photocatalytic reaction. Those features will be discussed in **Chapter 3**.

1-6 Effect of Co-catalyst in Photocatalysis

A term "co-catalyst" has been commonly used in the field of photocatalysis, though its definition seems ambiguous. In general, modifiers, especially fixed on the surface of photocatalysts, which enhance photocatalytic activities, i.e., the rate is increased by the

loading of which, and are expected not to work as a photocatalyst are called co-catalyst.

In the early stage of photocatalysis studies, it was found that loading of platinum on the surface of photocatalyst particles enables hydrogen evolution from water in the presence of electron donors such as methanol and EDTA and platinum has been assigned to be "hydrogen-evolution co-catalyst". Since hydrogen overpotential, excess potential needed to induce hydrogen evolution on an electrode, of metal oxides such as titania is reported to be large, hydrogen evolution does not proceed even if the CB bottom position is higher than the standard electrode potential for hydrogen evolution ($2H^+ + 2e^- = H_2$; 0 V (as a definition)) and platinum with almost zero hydrogen overpotential works as a catalyst to enhance hydrogen evolution [Baba 1985]. In the other words, platinum reduces activation energy for electron transfer from a photocatalyst to proton, an substrate, i.e., the rate constant of this electron transfer step in a possible kinetic model is increased by platinum loading. For the reported co-catalysts for oxygen evolution, e.g., cobalt phosphate [Kanan 2008] and manganese oxide [Li 2013], similar activation-energy reduction might happen. However, at the same time, a term "electron pool" has also been used to describe the action of platinum on the photocatalyst surface, as a different meaning of the above-mentioned "co-catalyst". This is less acceptable when kinetic model is proposed for the platinum-loaded photocatalysts; assumption of electron accumulation in platinum deposits is inconsistent with the probable catalytic action, i.e., fast consumption of electron to yield hydrogen. In addition to platinum [Sato 1980], rhodium [2006 Maeda] and iridium [Inoue 1994] were also reported to be a co-catalyst for hydrogen evolution.

Recently, especially from the beginning of the 2000's, the role of co-catalysts have been described as "enhancement of charge separation (of photoexcited electrons and positive holes)" or simply "prevention of recombination" by capturing charges, photoexcited electrons and/or positive holes [Maeda 2010/Yang 2013]. However, there seemed to be no reports showing the direct proof for this proposal and measurement of recombination rate. What we can see in the experimental results is just how much percentage of electron-positive hole pairs are not used for a given photocatalytic reaction by subtracting percentage of utilized pairs from 100 on the basis of product analysis. Even if the percentage of utilized pairs is increased, its reason can be acceleration of reaction of charges with substrates, but not limited to retardation of recombination, i.e., "enhanced charge separation" is almost identical to "the overall rate is increased", i.e., only telling the resultant utilization efficiency.

Another significant point in the discussion of co-catalyst effect is the possible backward reaction on the surface of co-catalyst. In the early 1980's, it has been reported that coating of platinum-loaded titania-photocatalyst surface by a sodium hydroxide layer enhances the water splitting into hydrogen and oxygen by retardation of backward dark reaction of once-evolved hydrogen and oxygen on the platinum surface keeping water as a substrate on the surface [Sato 1980], suggesting that for energy-storing photocatalytic

reaction in which a backward reaction is spontaneous such prevention of backward reactions is necessary. Recent reports also indicated that coating of co-catalyst surface enhances overall reaction, e.g., a nickel oxide layer on nickel co-catalyst [2001 Zou] and chromium oxide-coated platinum, rhodium and lanthanide nanoparticles in the so-called core-shell structure [Maeda 2006/Wang 2014].

For the clarification of true mechanism of co-catalyst action in photocatalysis, the previously proposed mechanistic models seems still ambiguous. Although some papers reported the spectroscopic studies on the co-catalytic action [Zhang 2014/Li 2006/Barosso 2014], it seems that we have few experimental techniques to obtain the proof even when the backward reaction is neglected.

1-7 Artificial Photosynthesis

It is well known that photosynthesis by natural plants is one of the largest scale chemical reaction occurring on the earth. In this reaction, photosynthesis, a series of photoinduced and dark reactions proceed to fix carbon dioxide (CO_2) (dark reaction) and water oxidation (light reaction) to produce glucose and oxygen, respectively. The overall reaction is shown as:

$$6CO_2 + 12H_2O \rightarrow C_6H_{12}O_6 + 6O_2 + 6H_2O. \quad (1)$$

The natural photosynthetic reaction center consists of photosystem II (PS II) catalyzing the photoinduced water oxidation and photosystem I (PS I) reducing carbon dioxide into glucose. It has been found that these reactions, initiated by photoabsorption of chlorophyll in plants, is driven by the catalytic action of manganese clusters in chlorophylls [Krishtalik 1986/Volkov 1986/Babcock 1989/Kamiya 2003/Ferraira 2004]. However, the detailed mechanism and precise structure of the photosynthetic reaction center has not yet been clarified.

In the early stage of photocatalysis studies, solar light-induced water splitting and carbon-dioxide fixation, mimicking the above-mentioned natural photosynthesis, was the main target and many researchers have been working to construct the system of "artificial photosynthesis", or such motivation to apply photocatalysis to produce fuels by solar-light irradiation and to solve the problem of energy shortage was the reason why the field of photocatalysis becomes much extended. The first report of water splitting using photoelectrochemical reaction was reported by Fujishima and Honda, initiating the boom of photocatalysis studies [Fujishima 1972]; a single-crystal titania electrode was UV-photoirradiated under electrical or chemical bias application to yield oxygen on the titania

electrode and hydrogen on a platinum counter electrode. Since then, many attempts to extend photoabsorption wavelength from UV to visible-light region which solar light mainly contains (ca. 50% [RREDC 1976]) and to improve the efficiency by doping heteroatoms in photocatalyst [Hameed 2004/Iwashina 2011/Kudo 2000/Liu 2006/Yang 2009] and loading of co-catalysts and/or metal complexes (or dyes) on the photocatalyst surface [Li 2013b/ DiSalle 2015] have been reported so far. The brief summary of these studies is described as follows.

1-7-1 Water Splitting in Photocatalysis

Splitting water into hydrogen and oxygen as one of the reaction of artificial photosynthesis has been studied by many researchers to improve the overall solar-energy conversion efficiency by extending the possible photoabsorption wavelength region and quantum efficiency as described in several recent reviews [Kudo 2008/Abe 2010/Maeda 2011]. As described in the preceding section, in the first report using titania as a semiconducting material only UV light could lead to the water splitting under appreciable electrical or chemical bias potential [Fujishima 1972]. Then, efforts to extend the photoabsorption wavelength to visible range have been made, but, in practice, it was rather difficult to construct the reaction syste satisfying both visible-light activity and high efficiency. One of the possible reasons is that almost all those studies were based on the design of band structure of photocatalysts adjusting the positions of VB top and CB bottom suitable for oxygen and hydrogen evolution reactions, respectively. According to the band-structure model as described in the previous section, band narrowing inducing visible-light absorption required anodic shift of CB bottom position, cathodic shift of VB top position or both. If the candidates of photocatalysts are limited to photostable simple or mixed metal oxides only, their VB top position seems almost fixed since VB predominantly consists of oxygen 2p orbitals, and thereby band narrowing may induce lowering CB bottom position not suitable for hydrogen evolution. The VB top position of metal sulfides and nitrides is expected to be higher than that of ordinary metal oxides and hence their CB bottom position could be higher than the standard electrode potential for hydrogen evolution. However, those metal sulfides and nitrides may undergo oxidative decomposition in the absence of electron donors to liberate oxygen from water.

In order to overcome the aforementioned problem, so-called Z-scheme type photocatalytic reaction systems have been developed; hydrogen and oxygen evolutions are performed using two kinds of photocatalysts and so-called redox mediator such as an iodate/iodide redox couple. This type of photocatalytic reaction system was reported in 1979 for the first time [Bard 1979]. The first report on Z-scheme photocatalytic water splitting was reported in 2001 [Sayama 2001], in which two different semiconductor photocatalysts and an iodate/iodide redox couple were used as shown in **Fig. 1-2**. This

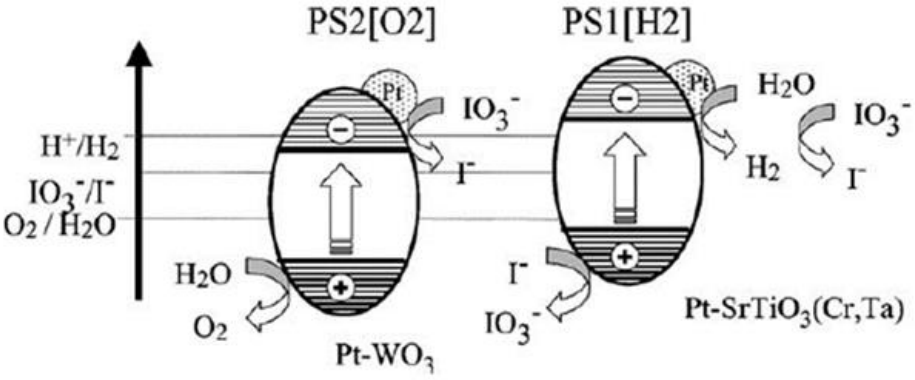

Fig. 1-2 Speculated reaction mechanism of Z-Scheme using an iodate(IO_3^-)/iodide (I^-) mediator
[Sayama 2001]

significant findings are applied for the development of photocatalysis designing as the new concepts and many researchers have investigated for development of visible light responsible water splitting system.

1-7-2 Photocatalytic Carbon-Dioxide Reduction

If the hydrogen-evolution half-cell reaction is substituted by carbon-dioxide reduction keeping the oxygen-evolution half-cell reaction the same, carbon-dioxide fixation using water as a reducing agent is achieved. Different from the water splitting into hydrogen and oxygen, carbon-dioxide reduction half-cell reaction can liberate several kinds of products. The corresponding standard electrode potentials are listed below (potentials are shown in reference to the potential of standard hydrogen electrode (SHE) [Bard 1985].

$$CO_2 + e^- = CO_2^{\bullet -} \quad (-1.90\ V) \quad (2)$$

$$CO_2 + 2H^+ + 2e^- = HCOOH \quad (-0.19\ V) \quad (3)$$

$$CO_2 + 2H^+ + 2e^- = CO + H_2O \quad (-0.10\ V) \quad (4)$$

$$CO_2 + 4H^+ + 4e^- = HCHO + H_2O \quad (-0.06\ V) \quad (5)$$

$$CO_2 + 6H^+ + 6e^- = CH_3OH + H_2O \quad (0.04\ V) \quad (6)$$

$$CO_2 + 8H^+ + 8e^- = CH_4 + 2H_2O \quad (0.18\ V) \quad (7)$$

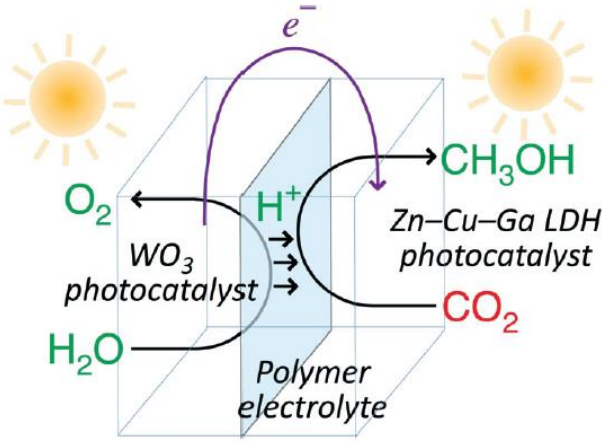

Fig. 1-3 Carbon dioxide-reduction system using double-layered photocatalyst device under visible-light irradiation [Morikawa 2014]

Except of one-electron reaction (**eq. 2**), all these electrode processes are multielectron transfer and only the potential of six and eight-electron processes (**eqs. 6** and **7**) is more anodic (positive) than that of hydrogen evolution. Therefore, those carbon dioxide-reduction processes are competitive to water reduction. In fact, it was impossible to avoid preferable production of hydrogen in the photocatalytic reaction systems in the presence of liquid water or water vapor.

In the first report on photoinduced carbon-dioxide reduction in an electrochemical system by Hemminger et al. [Hemminger 1978], it was shown that methane was liberated from water vapor and carbon dioxide under mercury-lamp UV irradiation. Then, Halmann reported the production of acetic acid, formaldehyde and methanol in the electrochemical system with a p-type gallium phosphate electrode [Halmann 1978]. The results of photocatalysis to yield formaldehyde and methanol in aqueous suspension of several kinds of photocatalyst powders were reported in 1979 [Inoue 1979]. Recent progress in photocatalytic carbon-dioxide reduction under visible-light irradiation has been reported for the systems containing a layered double hydroxide photocatalyst [Morikawa 2014] (**Fig. 1-3**), ruthenium-rhenium-complex adsorbed on a photoelectrode [Sahara 2016] and the above-mentioned Z-scheme photocatalytic reaction systems [Sato 2011/Sekizawa 2013/Kuriki 2016/Suzuki 2018]

1-8 Thermodynamics of Multielectron Process in Photocatalysis

1-8-1 Standard Electrode Potential

Thermodynamics of photocatalysis is, in principle, discussed using standard electrode potentials (SEPs) of reaction substrates in relation with the CB bottom and VB top positions of a photocatalyst as described in **Section 1-1**. SEP is defined as electrode potential in a given half-cell containing a redox couple in an electrolyte being in electrochemical equilibrium with a virtual electrode in which all the components (including electrons) have activity (concentration) of unity (1 mol kg^{-1}) (For electrons in a conductive electrode activity is defined as unity.), and if, e.g., proton is included in a redox couple, the corresponding SEP is defined at pH = 0. Thus, the term "standard" in SEP shows this activity of unity. In this definition, "electrochemical equilibrium" means that forward and backward electron transfer occurs, but their absolute value of forward and backward current is the same to result in no net current. This seems that an electrode in the SEP definition is virtual without any characteristics and inputting and outputting of electrons to/from the electrode are every time guaranteed in the definition of SEP. The most significant points is that the SEP definition consists of analogue values of activities of components including in a given equilibrium except for number of electrons transferred, which is digital as discussed in the following section.

1-8-2 Standard Electrode Potentials Related to Water Oxidation

As mentioned in the previous sections, water splitting into hydrogen and oxygen and carbon-dioxide reduction have been studied as an artificial photosynthesis. Oxygen evolution from water is included commonly in these reactions. In those works, it has been commonly presumed that four electrons are transferred from water to a photocatalyst, i.e., four positive holes are transferred from a photocatalyst to water. The corresponding SEP is shown below (According to the definition of SEP, electron must be on the left side, but these equations do not mean reduction. They are "equilibrium".), where SEP is shown in reference to SHE, as one of the possible equilibria of water oxidation [Bard 1985].

$$O_2 + 4H^+ + 4e^- = 2H_2O \quad (1.23\ V) \quad (8)$$

$$H_2O_2 + 2H^+ + 2e^- = 2H_2O \quad (1.76\ V) \quad (9)$$

$$\bullet OH + H^+ + e^- = H_2O \quad (2.8\ V) \quad (10)$$

The other two or one-electron transfer equilibria can also be assumed (**eqs. 9** and **10**) and those potentials are more anodic than that of four-electron transfer, i.e., those lower-number

transfer requires higher energy than four-electron transfer. Although the four-electron process have been and will be assumed if the observed actual product from water is oxygen, hydrogen peroxide (**eq. 9**) and hydroxyl radical (**eq. 10**) can be further oxidized to finally oxygen and therefore it cannot be concluded the four-electron transfer process only by oxygen detection. For example, oxidation of hydrogen peroxide into oxygen in two-electron transfer process has more cathodic SEP than hydrogen-peroxide liberation from water (**eq. 9**) as,

$$O_2 + 2H^+ + 2e^- = H_2O_2 \quad (0.70\ \text{V}). \quad (11)$$

Therefore, if hydrogen peroxide is liberated from water in two-electron process (**eq. 9**), the once-produced hydrogen peroxide can be easily oxidized into oxygen in the above two-electron process (**eq. 11**).

Then, how can we determine the number of transferred electrons in the first step of water oxidation? In the electrochemical system using an electrode, it would be possible by measuring the actual electrode potential under working conditions. For example, if oxygen-evolution (or water-oxidation) current rise is observed at potential of 2.0 V and1.5 V (vs. SHE), one-electron process and two-electron process are excluded, respectively, since those processes cannot proceed at those potentials. This can be extended to photocatalysis, even though the potential of photocatalyst particles cannot be defined and measured; if a photocatalyst being active for oxygen evolution has its VB-top position at 2.0 V and 1.5 V, one-electron process and two-electron process are excluded similarly. However, as far as the author knows, there have been found no metal-oxide (nitride or sulfate) photocatalysts having VB-top position more cathodic than 1.5 V (vs. SHE), and therefore it seems that we cannot decide the number of transferred electrons, two or four, in the first step of photocatalytic oxygen evolution.

Multielectron transfer is one of the most significant features of heterogeneous photocatalysis, since only one electron is transferred, in principle, in homogeneous photocatalysis using molecules and metal complexes which cannot absorb multiple photons under ordinary continuous-light irradiation [Inoue 2011]. Actually, multielectron (positive hole) transfer such as oxygen evolution happens in heterogeneous photocatalysis. However, it seems that nobody knows how many electrons are transferred between a photocatalyst and a substrate.

1-9 Kinetics of Multielectron Process in Photocatalysis

As discussed in the preceding section, thermodynamic approach, though SEP itself is a thermodynamic parameter, may not give a clear answer for number of electrons in photocatalytic multielectron transfer processes. This may be caused by the definition of SEP; as mentioned in **Section 1-8-1**, any number of electrons can be transferred (in an equilibrium), i.e., multielectron transfer is always guaranteed in the concept of SEP. However, it is clear, for heterogeneous photocatalysis, e.g., four electron-transfer oxidation of water may not happen if only one photoexcited electron or positive hole is there in one photocatalyst particle. Then, one of the possible non-thermodynamic solutions is analyze photocatalytic reactions kinetically using a model derived taking number of electrons or positive holes accumulated in a photocatalyst particle into account.

1-9-1 Light Intensity-dependence Analysis in Photocatalysis

In both heterogeneous and homogeneous photocatalysis, absorption of a photon (or photons) is the first step followed by redox reactions of excited electrons (LUMO electron) and positive holes (HOMO vacancy) with substances. Therefore, reaction rate (r) of a photocatalytic reaction may be described as a function of light flux, i.e., rate of light incidence, in the unit of mol s^{-1} or W (= J s^{-1}), and generally expressed using a rate constant (a), light intensity (I) and intensity-dependence order (n) as follows,

$$r = a \times I^{n}. \quad (12)$$

This equation does not reflect any features of heterogeneous photocatalysis and not contain a concept of electron (positive hole) accumulation in each photocatalyst particle.

Several papers have been published and reported the studies on light-intensity dependence of the rate of heterogeneous photocatalysis. For photocatalytic organics decomposition reactions, it has been claimed that the overall reaction rate was proportional to square-root of light intensity, i.e., $n = 0.5$ [Kato 1964/Okamoto 1985/Ohko 1998/Torimoto 2004]. Although some reports claimed the 0.5th dependence was attributable to recombination of electrons and positive holes in each photocatalyst particle accelerated by higher intensity-light irradiation [Okamoto 1985], a kinetic model including radical-chain reaction with alkyl peroxy radical as a chain carrier seemed more plausible for the reactions under aerobic conditions [Kato 1964, Ohko 1998, Torimoto 2004]; the proposed peroxy radicals might undergo bimolecular termination reaction more accelerated under high-intensity irradiation. This was supported by linear light-intensity dependence (n = 1) for hydrogen evolution under deaerated conditions using the same titania photocatalyst powders [Torimoto 2004]. Anyway, in those studies, number of accumulated electrons was not

taken into consideration (The former claim of accelerated recombination assumed the presence of many electrons and positive holes to obey second order-rate process, but not the number was not counted or counted as analogue value.).

A recent report on visible-light (green LED) induced photocatalysis by gold nanoparticle-deposited titania for oxidative decomposition of formic acid has shown that the order of light-intensity dependence was 1.87, almost two, and suggested two-photon gold-plasmonic absorption by each gold nanoparticle activating the photocatalyst [Tanaka 2013]. Similar possibility of two-photon absorption by gold particles has been also suggested [Kowalska 2010]. In those studies, however, the number of photons absorbed at the same time (or within the lifetime of excited state) was not counted, though multiphoton absorption in each particle leading to creation of multiple charge carriers was assumed.

Thus, historically, several studies on heterogeneous photocatalysis kinetically analyzed the mechanism on the basis of light-intensity dependence taking into account the number of accumulated electrons or positive holes, though the numbers were counted as analogue values. As claimed in **Section 1-8-1**, number of transferred electrons in water oxidation appearing in the SEPs is of digital value. Therefore, if the number is changed, depending on the reaction conditions, the rate must be changed in the fashion which is different from that in the ordinary kinetics using only parameters of analogue values. It is, then, expected that the rate of photocatalytic oxygen evolution obeys "digital" kinetics, not the conventional "analogue" kinetics.

1-10 Kinetic Analysis on Multielectron Transfer in Heterogeneous Photocatalysis–The Purpose of Present Study

Artificial photosynthesis is one of the most significant applications of homogeneous and heterogeneous photocatalysis, which may solve the energy-shortage problem on the earth, and the most studied two types of artificial photosynthetic reactions, water splitting and carbon-dioxide reduction, involves a process of oxygen liberation from water through multielectron-transfer processes (Carbon-dioxide reduction is also multielectron transfer reaction.). Such multielectron transfer requires multiphoton absorption in one unit of a photocatalyst, a molecule (or a metal complex) and a photocatalyst particle in homogeneous and heterogeneous photocatalysis, respectively. Under the ordinary continuous photoirradiation, only photocatalyst particles may satisfy this requirement, while the probability of multiphoton absorption by a molecule is negligible. Oxygen evolution from water, a reversed reaction of reduction of oxygen into water, is the most fundamental multielectron redox reaction and most largely occurring chemical reaction on the earth as a part of natural photosynthesis. It is well known that this reaction proceeds in heterogeneous

photocatalytic reaction systems and many studies have been performed. However, as mentioned in the previous sections, the number of electrons transferred (or, which SEP is adopted) in the first step of reaction has not been clarified, i.e., the most important point in its mechanism has not been disclosed yet.

Although several studies on this photocatalytic oxygen evolution from water discussed on the basis of transient absorption measurement [Tang 2013/Formal 2015/Mohamed 2011/Cowan 2013] or in-situ FT-IR absorption spectrometric analysis on the photocatalyst surface [Nakabayashi 2013, Nakamura 2003] claimed the reaction mechanism, there seemed no insights related to the number of transferred electrons, and so did the other so many reported studies on, e.g., the effect of modification of photocatalyst by doping or co-catalyst deposition, correlation between the reaction efficiency and physical properties such as crystallinity, crystalline form, specific surface area and so on.

The study in this thesis aims at clarifying the number of transferred electrons in heterogeneous photocatalytic oxygen evolution reaction systems, as the most significant parameter in the mechanism, using various titania powders as a photocatalyst through kinetic analysis based on light-intensity dependence of photocatalytic reaction rate and a kinetic model taking into account of the number of accumulated electrons in each particle, as digital value, as a novel concept of chemical kinetics.

Following this chapter (**Chapter 1**) thus-describing the background of studies, experimental and kinetic analytical methods and procedures are described in **Chapter 2**, and then **Chapters 3** and **4** contain results and discussion on the kinetic analysis. In **Chapter 3**, light-intensity dependence of the rate of oxygen evolution from the suspensions of several kinds of titania powder and electron acceptors under the monochromatic UV irradiation using highly intense UV-LEDs is presented as the first report on this measurement. The observed variation in the number of light-intensity dependence, depending on the kinds of titania photocatalysts, electron acceptors and light intensity, is discussed using a novel kinetic model involving the number of accumulated electrons in each photocatalyst particle. The estimated number of transferred electrons is suggested. On the basis of the above-mentioned results and discussion, the role of co-catalysts, which has not been clarified yet, is discussed in **Chapter 4**. In the light intensity-dependence analysis, variation in the rate enhancement of the titania photocatalyzed oxygen evolution and the order of light-intensity dependence was observed depending on the kinds of co-catalysts and their deposited amount. These results provide a novel insight on the role of co-catalyst. Then, conclusions based on the whole results and discussion and future aspects are described in **Chapter 5** to complete the study in this thesis.

1-11 References

[Abe 2010] Abe, R., Recent progress on photocatalytic and photoelectrochemical water splitting under visible light irradiation, *J. Photochem. Photobiol. C: Photochemistry Reviews* , **11**, 179–209 (2010).

[Baba 1985] Baba, R.; Nakabayashi, S.; Fujishima, A.; Honda, K., Investigation of the mechanism of hydrogen evolution during photocatalytic water decomposition on metal-loaded semiconductor powders, *J. Phys. Chem.*, **89**, 1902–1905 (1985).

[Babcock 1989] Babcock, G.T., Barry, B.A., Debus, R.J., Hoganson, C.W., Atamian, M., Mclntosh, L., Sithole, I., Yocum, C.F., Water Oxidation in Photosystem II: From Radical Chemistry to Multielectron Chemistry. *Biochemistry*, **28**, 9557–9565 (1989).

[Bard 1979] Bard, A. J., Photoelectrochemistry and Heterogeneous Photocatalysis at Semiconductors, *J. Photochem.*, **10**, 59–75 (1979).

[Bard 1985] Bard, A. J.; Parsons, R.; Jordan, J., Standard Potentials in Aqueous Solution, *Marcel Dekker*, New York and Basel (1985).

[Barosso 2014] Barroso, M., Cowan, A. J., Pendlebyry, S. R., Gratzel, M., Klug, D. R., Durrant, J.R., The Role of Cobalt Phosphate in Enhancing the Photocatalytic Activity of α-Fe_2O_3 toward Water Oxidation, *J. Am. Chem. Soc.*, **133**, 14868−14871 (2011).

[Cowan 2013] Cowan, A. J., Tang, J., Leng, W., Durrant, J. R., Water Splitting by Nanocrystalline TiO_2 in a Complete Photoelectrochemical Cell Exhibits Efficiencies Limited by Charge Recombination, *J. Phys. Chem. C*, **114**, 4208–4214 (2010).

[Disalle 2015] Disalle, B.F., Bernhard, S., Orchestrated Photocatalytic Water Reduction Using Surface-Adsorbing Iridium Photosensitizers, *J. Am. Chem. Soc.*, **133**, 11819−11821 (2011).

[Ferreira 2004] Ferreira, N.K., Iverson, T.M., Maghlaoui, K., Barber, J., Iwata, S. Architecture of the Photosynthetic Oxygen-Evolving Center. *Science* **303**, 1831–1838 (2004).

[Formal 2015] Formal, F. L., Pastor, E., Tilley, S. D., Mesa, C. A., Pendlebury, S. R., Gratzel, M., Durrant, J. R., Rate Law Analysis of Water Oxidation on a Hematite Surface, *J. Am. Chem. Soc.*, **137**, 6629−6637 (2015).

[Fujihara 2000] Fujihara, K., Izumi, S., Ohno, T., Matsumura, M., Time-resolved photoluminescence of particulate TiO_2 photocatalysts suspended in aqueous solutions. *J. Photochem. Photobiol. A: Chem.*, **132**, 99–104 (2000).

[Fujihara 1998] Fujihara, K., Ohno, T., Matsumura, M., Splitting of water by electrochemical combination of two photocatalytic reactions on TiO2 particles. *J. Chem. Soc., Faraday Trans.*, **94**, 3705–3709 (1998).

[Fujishima 1972] Fujishima, A., Honda, K., Electrochemical Photolysis of Water at a Semiconductor Electrode, *Nature*, **238**, 37–38 (1972).

[Hameed 2004] Hameed, A., Gondal, M., A., Yamani, Z.H., Effect of transition metal doping on photocatalytic activity of WO_3 for water splitting under laser illumination: role of 3d-orbitals, Catalysis Communications, **5**, 715-719 (2004).

[Halmann 1978] Halmann, M., Photoelectrochemical reduction of aqueous carbon dioxide on p-type gallium phosphide in liquid junction solar cells, *Nature*, **175**, 115–116 (1978).

[Hemminger 1978] Hemminger, J.C., Carr, R., Somorjai, G.A., The Photoassisted Reaction of Gaseous Water and Carbon Dioxide Adsorbed on the $SrTiO_3$ (111) Crystal Face to Form Methane, *Chem. Phys. Lett.*, **57**, 100–104 (1978).

[Hong 2012] Hong, D., Yamada, Y., Nagatomi, T., Takai, Y., Fukuzumi, S., Catalysis of Nickel Ferrite for Photocatalytic Water Oxidation Using $[Ru(bpy)3]^{2+}$ and $S_2O_8^{2-}$, *J. Am. Chem. Soc.*, **134**, 19572-19575 (2012).

[Inoue 1979] Inoue, T., Fujishima, A., Konishi, S., Honda, K., Photoelectrocatalytic reduction of carbon dioxide in aqueous suspensions of semiconductor powders, Nature, 637–638 (1979).

[Inoue 1994] Inoue, Y., Asai, Y., Sato, K., Photocatalysts with Tunnel Structures for Decomposition of Water Part 1.- $BaTi_4O_9$, a Pentagonal Prism Tunnel Structure, and its Combination with various Promoters, *J. Chem. Soc. Faraday Trans.*, **98**, 797–802 (1994).

[Inoue 2011] Inoue, H., Shimada, T., Kou, Y., Nabetani, Y., Masui, D., Takagi, S., Tachibana, H., The Water Oxidation Bottleneck in Artificial Photosynthesis: How Can We Get Through It? An Alternative Route Involving a Two-Electron Process, *ChemSusChem*, 173–179 (2011).

[Iwashina 2011] Iwashina, K., Kudo, A., Rh-Doped $SrTiO_3$ Photocatalyst Electrode Showing Cathodic Photocurrent for Water Splitting under Visible-Light Irradiation, *J. Am. Chem. Soc.*, **133**, 13272−13275 (2011).

[Kamiya 2003] Kamiya, N., Shen, J. R., Crystal structure of oxygen-evolving photosystem II from Thermosynechococcus vulcanus at 3.7-Å resolution. *Proc. Natl. Acad. Sci. U.S.A.* **100**, 98–103 (2003).

[Kanan 2008] Kanan, W. M., Surendranath, Y., Nocera, G.D., Cobalt-phosphate oxygen-evolving compound, *Chem. Soc. Rev.*, **38**, 109–114 (2009).

[Kato 1964] Kato, M., Masuo, F., *Kogyo kagaku Zasshi*, **67**, 1136–1140 (1964).

[Kavan 1996] Kavan, L., Graetzel, M., Gilbert, S. E., Klemenz, C., Scheel, H. J., Electrochemical and Photoelectrochemical Investigation of Single-Crystal Anatase, *J. Am. Chem. Soc.*, **118**, 6716–6723 (1996).

[Kowalska 2010] Kowalska, E.; Prieto-Mahaney, O.-O.; Abe, R.; Ohtani, B., Visible-light-induced photocatalysis through surface plasmon excitation of gold on titania surfaces, *Phys. Chem. Chem. Phys.*, **12**, 2344–2355 (2010).

[Krishtalik 1986] Krishtalik, L. I., Energetics of multielectron reactions. Photosynthetic oxygen evolution. *Biochimica et Biophysica Acta*, **849**, 162–171 (1986).

[Kudo 2000] Kudo, A., Kato, H., Effect of lanthanide-doping into $NaTaO_3$ photocatalysts for effcient water splitting, *Chem. Phys. Lett.*, **331**, 373-377 (2000).

[Kudo 2008] Kudo, A., Miseki, Y., Heterogeneous photocatalyst materials for water splitting, *Chem. Soc. Rev.*, **38**, 253-278 (2009).

[Kuriki 2016] Kurii, R., Matsunaga, H., Nakashima, T., Wada, K., Yamakata, A., Ishitani, O., Maeda, K., Nature-Inspired, Highly Durable CO_2 Reduction System Consisting of a

Binuclear Ruthenium (II) Complex and an Organic Semiconductor Using Visible Light, *J. Am. Chem. Soc.*, **138**, 5159-5170 (2016).

[Li 2007] Li, H., Bian, Z., Zhu, J., Huo, Y., Li, H., Lu, Y., Mesoporous Au/TiO_2 Nanocomposites with Enhanced Photocatalytic Activity, *J. Am. Chem. Soc.*, **129**, 4538−4539 (2007).

[Li 2015] Li, R., Weng, Y., Zhou, X., Wang, X., Mi, Y., Chong, R., Han, H., Li, C., Achieving overall water splitting using titanium dioxide-based photocatalysts of different phases, *Energy Environ. Sci.*, **8**, 2377–2382 (2015).

[Li 2013a] Li, R., Zhang, F., Wang, D., Yang, J., Li, M., Zhu, J., Zhou, X., Han, H., Li, C., Spatial separation of photogenerated electrons and holes among {010} and {110} crystal facets of $BiVO_4$, *Nature Commun.* , **4**, 1432–1439 (2013).

[Li 2013b] Li, M., Luo, W., Cao, D., Zhao, X., Li, Z., Yu, T. Zou, Z., A Co-catalyst-Loaded Ta_3N_5 Photoanode with a High Solar Photocurrent for Water Splitting upon Facile Removal of the Surface Layer, *Angew. Chem. Int. Ed.*, **52**, 11016-1102 (2013)

[Liu 2006] Liu, J. W., Chen, G., Li, Z. H., Zhang, Z. G., Electronic structure and visible light photocatalysis water splitting property of chromium-doped $SrTiO_3$, *J. Solid State Chem.*, **179**, 3704-3708 (2006).

[Maeda 2006] Maeda, K., Teramura, K., Lu, D., Saito, N., Inoue, Y., Domen, K., Noble-Metal/Cr_2O_3 Core/Shell Nanoparticles as a Cocatalyst for Photocatalytic Overall Water Splitting, *Angew. Chem. Int. Ed.*, **45**, 7806 –7809 (2006).

[Maeda 2010] Maeda, K., Domen, K., Photocatalytic Water Splitting: Recent Progress and Future Challenges, *J. Phys. Chem. Lett.*, **1**, 2655–2661 (2010)

[Maeda 2011] Maeda, K., Photocatalytic water splitting using semiconductor particles: History and recent developments, *J. Photochem. Photobiol. C: Photochemistry Reviews*, **12**, 237–268 (2011).

[Mills 1982] Mills, A., Porter, G., Photosensitised Dissociation of Water using Dispersed Suspensions of n-Type Semiconductors, *J. Chem. Soc. Faraday Trans 1* , **78** , 3659–3669 (1982)

[Mohamed 2011] Mohamed, H. H., Mendive, C. B., Dillert, R., Bahnemann, D. W., Kinetic and Mechanistic Investigations of Multielectron Transfer Reactions Induced by Stored Electrons in TiO_2 Nanoparticles: A Stopped Flow Study, *J. Phys. Chem. C*, **115**, 2139–2147 (2011).

[Morikawa 2014] Morikawa, M., Ogura, Y., Ahmed, N., Kawamura, S., Mikami, G., Okamoto, S., Izumi, Y., Photocatalytic conversion of carbon dioxide into methanol in reverse fuel cells with tungsten oxide and layered double hydroxide photocatalysts for solar fuel generation, *Catal. Sci. Technol.*, **4**, 1644–1651 (2014).

[Nakabayashi 2013] Nakabayashi, Y., Nosaka, Y., OH Radical Formation at Distinct Faces of Rutile TiO_2 Crystal in the Procedure of Photoelectrochemical Water Oxidation, *J. Phys. Chem. C*, **117**, 23832–23839 (2013).

[Nakamura 2003] Nakamura, R., Nakato, Y., Primary Intermediates of Oxygen Photoevolution Reaction on TiO_2 (Rutile) Particles, Revealed by in Situ FTIR Absorption and Photoluminescence Measurements, *J. Am. Chem. Soc.*, **126**, 1290−1298 (2004).

[Ohko 1998] Ohko, Y., Tryk, A. D., Hashimoto, K., Fujishima, A., Autooxidation of Acetaldehyde Initiated by TiO_2 Photocatalysis under Weak UV Illumination, *J. Phys. Chem. B*, **102,** 2699–2704 (1998).

[Ohtani 2014] Ohtani, B., Revisiting the Fundamental Physical Chemistry in Heterogeneous Photocatalysis: Its Thermodynamics and Kinetics, *Phys. Chem. Chem. Phys.*, **16**, 1788–1797 (2014).

[Okamoto 1985] Okamoto, K., Yamamoto, Y., Tanaka, H., Itaya, A., Kinetics of Heterogeneous Photocatalytic Decomposition of Phenol over Anatase TiO_2 Powder, *Bull. Chem. Soc. Jpn.*, **58**, 2023–2028 (1985).

[Ozawa 2007] Ozawa, K., Emori, M., Yamamoto, S., Yukawa, R., Yamamoto, S., Hobara, R., Fujikawa, K., Sakama, H., Matsuda, I., Electron−Hole Recombination Time at TiO_2 Single-Crystal Surfaces: Influence of Surface Band Bending, J. Phys. Chem. Lett. **5**, 1953−1957 (2014).

[Paola 2007] Paola, A.D, Cufalo, G., Addamo, M., Bellardita, M., Campostrini, R., Ischia, M., Ceccato, R., Palmisano, L., Photocatalytic activity of nanocrystalline TiO_2 (brookite, rutile and brookite-based) powders prepared by thermohydrolysis of $TiCl_4$ in

aqueous chloride solutions, *Colloids and Surfaces A: Physicochem. Eng. Aspects*, **317**, 366–376 (2008).

[Puntriero 2010] Puntoriero, F., Ganga, G. L., Sartorel, A., Carraro, M., Scorrano, G., Bonchio, M., Campagna, S., Photo-induced water oxidation with tetra-nuclear ruthenium sensitizer and catalyst: A unique 4 x 4 ruthenium interplay triggering high efficiency with low-energy visible light, *Chem. Commun.*, **46**, 4725-4727 (2010)

[Roger 1990] Bickley, R. I., Gonzalez-Carreno, T., Lees, J. S., Palmisano, L., Tilley, R. J. D., A Structural Investigation of Titanium Dioxide Photocatalysts, *J. Solid State Chem.* **92**, 178-190 (1991).

[RREDC 1976] The Renewable Resource Data Center (RReDC), The government of United States of America, Reference Solar Spectral Irradiance: Air Mass 1.5, http://rredc.nrel.gov/solar/spectra/am1.5/

[Sahara 2016] Sahara, G., Kumagai, H., Marda, K., Kaeffer, N., Artero, V., Higashi, M., Abe, R., Ishitani, O., Photoelectrochemical Reduction of CO_2 Coupled to Water Oxidation Using a Photocathode with a Ru(II)−Re(I) Complex Photocatalyst and a CoOx/TaON Photoanode, *J. Am. Chem. Soc.*, **138**, 14152−14158 (2016).

[Sato 1980] Sato, S., White, J. M., Photodecomposition of Water over Pt/TiO_2 Catalysts, *Chem. Phys. Lett.*, **72**, 83–86 (1980).

[Sato 2011] Sato, S., Arai, T., Morikawa, T., Uemura, K., Suzuki, M. T., Tanaka, H., Kajino, T., Selective CO_2 Conversion to Formate Conjugated with H_2O Oxidation Utilizing Semiconductor/Complex Hybrid Photocatalysts *J. Am. Chem. Soc.*, **133**, 15240−15243 (2011).

[Sayama 2001] Sayama, K. Mukasa, K., Abe, R., Abe, Y., Arakawa, H., Stoichiometric water splitting into H_2 and O_2 using a mixture of two different photocatalysts and an IO_3^-/I^- shuttle redox mediator under visible light irradiation, *Chem. Commun.*, 2416–2417 (2001).

[Sekizawa 2013] Sekizawa, K., Maeda, K., Domen, K., Koike, K., Ishitani, O., Artificial Z‐Scheme Constructed with a Supramolecular Metal Complex and Semiconductor for the Photocatalytic Reduction of CO_2, *J. Am. Chem. Soc.*, **135**, 15240−15243 (2011).

[Suzuki 2018] Suzuki, M. T., Takayama, T., Sato, S., Kudo, A., Morikawa, T., Enhancement of CO_2 reduction activity under visible light irradiation over Zn-based metal sulfides by combination with Ru-complex catalysts, *Appl. Catal. B: Environmental*, **224**, 572–578 (2018).

[Tanaka 2013] Tanaka, A., Hashimoto, K., Ohtani, B., Kominami, H., Non-linear photocatalytic reaction induced by visible-light surface-plasmon resonance absorption of gold nanoparticles loaded on titania particles, *Chem. Commun.*, **49**, 3419–3421 (2013).

[Tang 2013] Tang, J., Durrant, J. R., Klug, D. R., Mechanism of Photocatalytic Water Splitting in TiO_2. Reaction of Water with Photoholes, Importance of Charge Carrier Dynamics, and Evidence for Four-Hole Chemistry, *J. Am. Chem. Soc.*, **130**, 13885−13891 (2008).

[Torimoto 2004] Torimoto, T., Aburakawa, Y., Kawahara, Y., Ikeda, S., Ohtani, B., Light intensity dependence of the action spectra of photocatalytic reactions with anatase titanimun(IV) oxide, *Chem. Phys. Lett.*, **392**, 220-224 (2004).

[Valdes 2007] Valdes, A., Qu, Z.-W., Kroes, G.-J., Rossmelsl, J., Norskov, J. K., Oxidation and Photo-Oxidation of Water on TiO_2 Surface, *J. Phys. Chem. C*, ***112***, 9872–9879 (2008**)**.

[Volkov 1986] Volkov, A.G., The Electrochemical Mechanism of Photosystem II Functioning in Chloroplasts. *J. Electroanal. Chem.*, **205**, 245-257 (1986).

[Wang 2014] Wang, Q., Hisatomi, T., Ma, S. S. K., Li, Y., Domen, K., Core/Shell Structured La- and Rh-Codoped $SrTiO_3$ as a Hydrogen Evolution Photocatalyst in Z‑Scheme Overall Water Splitting under Visible Light Irradiation, *Chem. Mater.*, **26**, 4144−4150 (2014).

[Yamakata 2015] Yamakata, A., Vequizo, J. J. M., Matsunaga, H., Distinctive Behavior of Photogenerated Electrons and Holes in Anatase and Rutile TiO_2 Powders, *J. Phys. Chem. C*, **119**, 24538−24545 (2015).

[Yang 2013] Yang, J., Wang, D., Han, H., Li, C., Roles of Cocatalysts in Photocatalysis and Photoelectrocatalysis, *Account of Chemical Research*, **46**, 1900-1909 (2013)

[Zhang 2014] Zhang, F., Yamakata, A., Maeda, K., Moriya, Y., Takata, T., Kubota, J., Teshima, K., Oishi, S., Domen, K., Cobalt-Modified Porous Single-Crystalline $LaTiO_2N$ for Highly Efficient Water Oxidation under Visible Light, *J. Am. Chem. Soc.*, **134**, 8348−8351 (2012).

[Zou 2001] Zou, Z., Ye, J., Sayama, K., Arakawa, H., Direct splitting of water under visible light irradiation with an oxide semiconductor photocatalyst, *Nature*, **414**, 625–627 (2001).

Chapter 2

Materials and Methods

2-1 Materials (photocatalyst and compounds)

Photocatalytic activity test performed using commercial photocatalysts and compounds. In this study, a titanium (IV) dioxide (TiO_2) powder, which was the most popular photocatalyst was used. There were several kinds of photocatalyst were used, MT-150A (Tayca, rutile), ST-G2 (Showa Denko Ceramics, rutile), and ST-01 (Ishihara Sangyo, anatase), Fluka (anatase). These suppliers and physical properties were organized as shown in **Table 3-1**. In addition, the two type of Strontium titanate ($SrTiO_3$), (Aldrich 696141-100G: 5 μm, Aldrich 517011-50G: < 100 nm) were used.

In this study, the aqueous of photocatalytic oxygen evolution were prepared using iron(III) chloride hexahydrate ($FeCl_3$ $6H_2O$; Kanto Chemical, iron(III) (Fe^{3+}) ion as an acceptor), or sodium iodate ($NaIO_3$; Wako Pure Chemical Industries, iodate (IO_3^-) ion as an acceptor) and carbonate pH standard solution (Wako Pure Chemical Industries).

The particle-size of TiO_2 samples were estimated from the specific surface area using following equations. Based on the assuming the shape of TiO_2 particle as a sphere, the number of 1g TiO_2 particle (N) was derived using the real density of TiO_2 particle (ρ : 4×10^{-6} / g m^{-3}) and particle-size (d), as shown,

$$N = 1/(\rho \times 4/3 \times \pi \times (d/2)^2 \quad (13)$$

and surface area of particle (σ) as

$$\sigma = 4 \times \pi \times (d/2)^2. \quad (14)$$

Specific surface area (S) was derived from multiple of N and σ, and the particle size (d) was calculated as shown below.

$$S = N \times \sigma = 6/(\rho \times d) \quad (15)$$

$$d = 1500/S \quad (16)$$

2-2 Method of Photocatalysis

2-2-1 Photocatalytic Oxygen Evolution in the Presence of Electron Acceptor

Photocatalytic oxygen evolution from water proceeds in the presence of electron acceptor. In this study, the two type of electron acceptors were selected, iodate (IO_3^-) and iron(III) ion (Fe^{3+}), which were generally used in photocatalysis. The concentration of sodium-iodate ($NaIO_3$) or iron (III) chloride-hexahydorate aqueous were 50 mmol L^{-1} for each systems. The pH of aqueous was 2 for Fe^{3+} system, and almost 10 which was adjusted by carbonate buffer solution in IO_3^- system. A 30 mg of photocatalyst was suspended in aqueous solution in a rectangular quartz cell. Air was purged off from the cell by argon-gas flowing through the suspensions at least 5 min, and the cell was tightly sealed with a rubber septum and parafilm to prevent a leakage of gas and/or contamination. Photoirradiation by UV-LEDs (NSL and HMP type, the property of each light source described in **chapter 3**) through a 1 cm-square aperture set in front of the cell was performed at room temperature (298 K) under magnetic stirring in order to make incident photons thoroughly absorbed by titania particles. Amount of gases in the head space of quartz cell were detected by using gas chromatograph. The reaction formula of photocatalytic oxygen evolution for Fe^{3+} and IO_3^- system were as shown here.

$$Fe^{3+} + e^- \rightarrow Fe^{2+} \qquad (17)$$

$$IO_3^- + 3H_2O + 6e^- \rightarrow I^- + 6OH^- \qquad (18)$$

$$O_2 + 4H^+ + 4e^- = 2H_2O \quad (1.23\ V) \quad (8)$$

In this study, It was not used the electron acceptor through metal deposition in reduction process e.g. silver (I) ion (Ag^+), because metal deposition on the surface could make the photoabsorption reducing and prevent to proceeding of photocatalytic reaction, and probably the negative effect of surface positive charging to keep away the absorption of Ag+ from photocatalyst surface [Nishimoto 1983]. Therefore, it is considered the kinetic analysis of oxygen evolution using electron acceptors without photodeposition.

In the case of Fe^{3+} system, iron (II) ion which is reduced product of Fe^{3+} were detected by 1,10-phenanthroline as an detection reagent. The aqueous of 1,10-phenanthroline poured to a supernatant of sample, and then photoabsorption spectrum was measured by UV-Vis Spectrophotomerer (SHIMADZU MPS-2450).

2-2-2 Gas Chromatography Measurement

Chromatography is one of the popular method for analysis of sample compounds

which are separated by the column with carrier gas/liquid flowing, and detected according to the retention time of each component peaks. Gas chromatograph (GC-8A, Shimadzu) with argon gas (Ar) carrier are generally used for gas composition analysis in photocatalysis. In this study, it was used argon gas as the carrier gas. The detector was thermal conductivity detector (TCD) to detect the separated components, which was directly connected to the carrier gas flowing line. The quantitative analysis was calculated from multiplies the peak area and the slope of calibrated curve for each component as shown below.

The condition of GC measurement was described below. The flow rate of Ar gas was 50 mL min^{-1} and the temperature of injection and detector were 100 and 80 degree Celsius, respectively. The column were used molecular sieves 5A which could detect hydrogen, oxygen, and nitrogen gaseous in sample air. In this analysis, 0.2 mL sample gaseous which were taken from quartz cell by micro syringe injected. Photocatalytic reaction rate were derived from the time course of evolved oxygen gases, and oxygen gas leakage from the air was subtracted with the amount of nitrogen multiplied the ratio of oxygen and nitrogen molecules in the air.

2-2-3 Gas Chromatography and Mass Spectroscopy Analyse

In general, it had been used the gas chromatograph and mass spectroscopy (GC-MS) for considering the isotope experiment to clarify the element source of products. In this study, it was discussed the oxygen-isotope experiment to analyze the source of oxygen molecules in the liberation of oxygen products. Oxygen-isotope experiments were performed using commercial TiO_2 sample suspended in a 75/25 ratio mixture of Milli-Q water ($H_2{}^{16}O$) and isotope-labeled water ($H_2{}^{18}O$; ≧99.8%, Taiyo Nippon Sanso) containing IO_3^- or Fe^{3+} ions as an EA. Liberated oxygen was analyzed by a gas chromatograph-mass spectrometer (Shimadzu GC-17A/GCMS-QP5050A). The atomic content of ^{18}O (^{18}O content) in liberated oxygen was calculated with the following equation; ^{18}O content = $1/(1 + (I_p(^{16}O^{18}O) / I_p(^{18}O_2))$, where $I_p(^{16}O^{18}O)$ and $I_p(^{18}O_2)$ are relative intensity of $^{16}O^{18}O$ (m/e = 34) and $^{18}O_2$ (m/e = 36) peak intensities on the assumption that $^{16}O_2$ was contaminated by air and $^{16}O_2$-peak intensity could not be used for calculation. The theoretical ^{18}O content was calculated by assuming the purity of the $H_2{}^{18}O$ to be 99.8% to be 0.245.

2-2-4 Calcination of TiO_2

The calcined TiO_2 sample was prepared by rotary furnace instrument which was constructed by the rotary unit of evaporator combined glasses and electric furnace. The rotary unit is contributed for the homogenious calcination the samples. The small rutile sample (MT-150A) was calcined at 873 K and rotated in 60 rpm. The physical properties of calcined sample were analyzed by XRD and BET measurement as described below.

2-2-5 X-ray Diffraction (XRD) Analysis

Crystalline (and non-crystalline) composition of samples was analyzed by X-ray diffractometry (XRD). In XRD measurement using a Rigaku SmartLab diffractometer, 0.300 g of a sample and 0.075 g of nickel oxide (NiO; Wako Pure Chemical) as an internal standard were mixed thoroughly in an agate mortar and set in a sample holder. The measurement conditions were as follows: an X-ray tube (copper Ka) operated at 40 kV and 30 mA; scanning rate of 1.0º min-1; step of 0.02º; and 2θ range of 3–80º. The acquired diffractograms were analyzed by software installed in the controlling personal computer (PDXL including a RIETAN-FP Rietveld analysis package). Based on the assumption that NiO is 100% crystalline, i.e., without a non-crystalline part, crystalline TiO_2 content was calculated from the results of Rietveld analysis.

2-2-6 Specific Surface Area Measurement by Nitrogen Adsorption Method

A sample (50 mg) evacuated at 473 K for 2 h as a pretreatment was used for measurement of nitrogen adsorption at 77 K on a Quantachrome (previously Yuasa Ionics) Autosorb-6 surface area and pore size analyzer. Specific surface area (SSA) was calculated from adsorption isotherms by the Brunauer–Emmett–Teller (BET) equation.

2-2-7 Irradiation Setups of UV-LED Lamp (Focused/Unfocused type UV-LED)

The light-intensity dependence analysis was discussed using high intense monochromatic UV-LED lamp (λ = 365 nm) to prevent the influence of irradiation wavelength dependence. In this study, two-type of UV-LED (NS Lighting ULEDN-101 (NSL) and Hamamatsu Photonics L11921-400 (HMP)) were used which had different light-focusing property. The maximum power of focused NSL and that of unfocused HMP incident light beams from those LEDs measured by a Hioki 3664 power meter with a 9742 optical sensor through a 1 cm-square aperture in front of a rectangular quartz cell were ca. 340 mW and 500 mW, respectively. Light intensities were adjusted by changing the LED-cell distance (NSL) or source power (HMP). Those maximum intensities were more than one-order of magnitude higher than those of UV light from ordinary mercury or xenon arc lamps (ca. several tens of mW cm^{-2}).

2-2-8 Photon Density Distribution Measurement and Correction of Focusing Property

According to above section, both UV-LEDs have the different focusing property on

high intense irradiation, therefore it is difficult to compare the light-intensity dependence of reaction rate directly because the light-intensity power meter can only display the integrated value of intensity in 1 cm^2. It suggests that the inhomogeneity cannot be reflected without correction. In this study, the different focus properties were corrected by photon density distributions for each LED. The distribution in the irradiated area were calculated using iris diaphragm attached 1 cm-square aperture. The correction of light-intensity inhomogeneity (especially in a focused NSL beam) was performed by measuring the effective irradiation area in the center part in a 1 cm-square aperture passing 95% power (A_{95}). Light intensity was measured for a 0.10 cm-diameter circle at the center and increasing with 0.1 cm-width concentric circle. The difference of each light-intensity divided by the coaxial 0.1 cm-width ring area, and derived the distribution. An effective irradiation area corresponding to the 95% of total light intensity was estimated from distribution, and then, corrected irradiation-light intensity (I_L/ mW cm^{-2}) was calculated from total power in 1 cm-square aperture (Pa / mW) by following equation:

$$I_L = 0.95Pa/A_{95}. \quad (19)$$

The observed reaction rate of oxygen evolution (Ra) was also applied this correction and the corrected reaction rate (r) derived from the equation :

$$r = 0.95Ra/A_{95} \quad (20)$$

2-2-9 Preparation of Co-catalyst Loaded Photocatalyst

2-2-9-1 Photodeposition Method

It is well known that photodeposition is a popular method to deposit the co-catalyst on the photocatalyst surface. Photodeposition proceeds through photocatalytic reaction. Photocatalyst powder suspending in metal complex (precusor) aqueous with electron acceptor or donor proceeded photocatalytic reaction under light irradiation. A metal complex and electron donor (or acceptor) in suspention are reduced and oxidized by excited electron and positive hole on the photocatalyst surface, and then, the complexes turn to metal nano-particle (or metal oxide species). In this study, the three kind of co-catalyst were deposited on TiO_2. The deposition process proceeded under Ar bubbling condition to purge the air. The test tube was irradiated under high pressure mercury lamp (λ >290 nm) with magnetic stirring. After light irradiation, the sample was collected by centrifugation and drying to remove supernatant.

2-2-9-2 Cobalt Phosphate Deposition

Cobalt phosphate (Co-Pi) was deposited using cobalt nitrate ($Co(NO_3)_2$) and phosphate buffer solution according to the literature [Wang 2012]. 0.291 g of Cobalt nitrate hexahydrate were dissolved in 50 mL Milli-Q water and 50 mmol L^{-1} $Co(NO_3)_2$ aqueous were prepared. Phosphate buffer solution were prepared were immixed of each aqueous of sodium dihydrogen phosphate (NaH_2PO_4) and disodium hydrogen phosphate (Na_2HPO_4). 0.156 g and 0.358 g of sodium dihydrogen phosphate dihydrate and disodium hydrogen phosphate dodecahydrate were dissolved in 0.1 L Milli-Q water to prepare 10 mmol L^{-1} NaH_2PO_4 and Na_2HPO_4 aqueous. A 100 mL of phosphate buffer solution were prepared by immixed 50 mL of NaH_2PO_4 aqueous and Na_2HPO_4 aqueous with adjusting the pH value at 7. Titanium dioxide (600 mg) were suspended in 28.5 mL buffer solution and 0.510 mL $Co(NH_3)_2$ precursor aqueous (0.1 % equivalent amount of TiO_2).

2-2-9-3 Iridium Oxide Deposition

1 g of sodium hexachloroiridate(III) n-Hydrate ($Na_3(IrCl_6)$・nH_2O, Wako Pure Chemical Industries Ltd., Iridium purity: 31.5~40.5 %) was dissolved in 25 mL Milli-Q water to prepare 0.0655 mmol L^{-1} aquaous [Iwase 2005]. 5 mmol L^{-1} sodium nitrate aquaous were confected from sodium nitrate (Wako Pure Chemical Indastries Ltd. >99.0 %) and 100 mL milli-Q water. Amount of 600 mg TiO_2 were suspended in 28.6 mL 0.02 mol L^{-1} $NaIO_3$-aqueous with the mixture of $Na_3(IrCl_6)$・nH_2O (40.84 μL) and sodium nitrate (5 mL) aqueous, and then, the sample was under irradiation.

2-2-9-4 Manganese Oxide Deposition

1 g of manganese dioxide tetrahydrate ($MnCl_2 \cdot 4H_2O$Kishida chemical Co. Ltd. >99.0%) were dissolved in 25 mL milli-Q water to prepare 0.2 mol L^{-1} $MnCl_2$ aquaous according to the literature [Li 2013]. Amount of 600 mg TiO_2 were suspended in 28.6 mL 0.02 mol L^{-1} $NaIO_3^-$ aqueous with the mixture of $Na_3(IrCl_6) \cdot nH_2O$ (40.84 μL) under mercury lamp irradiation.

2-10 References

[Iwase 2005] Iwase, A., Kato, H., Kudo, A., A Novel Photodeposition Method in the Presence of Nitrate Ions for Loading of an Iridium Oxide Cocatalyst for Water Splitting, *Chem. Lett.*, **34**, 946-947 (2005).

[Li 2013] Li, R., Zhang, F., Wang, D., Yang, J., Li, M., Zhu, J., Zhou, X., Han, H., Li, C., Spatial separation of photogenerated electrons and holes among {010} and {110} crystal facets of $BiVO_4$, *Nature Commun.*, **4**, 1432-1439 (2013).

[Nishimoto 1983] Nishimoto, S., Ohtani, B., Kajiwara, H., Kagiya, T., Photoinduced Oxygen Formation and Silver-metal Deposition in Aqueous Solutions of Various Silver Salts by Suspended Titanium Dioxide Powder, *J. Chem. Soc. Faraday Trans.1*, **79**, 2685-2694 (1983).

[Wang 2012] Cobalt Phosphate–ZnO Composite Photocatalysts for Oxygen Evolution from Photocatalytic Water Oxidation, *Ind. Eng. Chem. Res.*, **51**, 9945−9951 (2012).

Chapter 3

Analysis of Light-intensity Dependence in Photocatalytic Oxygen Evolution

3-1 Introduction

Photocatalytic oxygen evolution from water is one of an important reaction for proceeding artificial photosynthesis. It has been discussed the factor to improve of

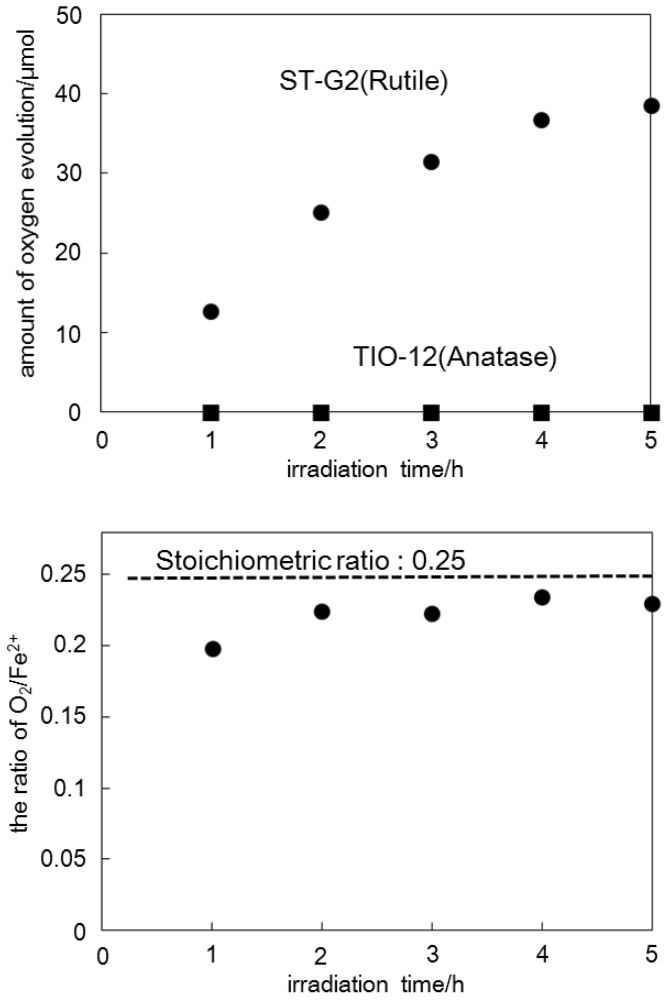

Fig.3-1 Time course of oxygen evolution under high-pressure mercury lamp and product ratio of Fe^{2+} ion and evolved oxygen using ST-G2 (rutile, 350 nm) and TIO-11(anatase, 15 nm) in the presence of Fe^{3+} as an acceptor

photocatalytic oxygen evolution reaction efficiency. As described in **chapter 1**, some reports indicate the effect of particle-size, electron acceptor which is a sacrificial reagent of an excited electron [Bamwenda 2001] and correlation of crystallinity of TiO_2 and electron acceptor [Ohno 1997/Fujihara 1998/Fujihara 2000/Ohno 2001]. In these case, it is discussed a reaction efficiency was depending on the photoabsorption efficiency according to particle-size, and the rate of the reversible reaction between a reduced product and positive hole. According to the discussion for influence of TiO_2 crystallinity as the preliminary experiments, higher reaction rate observed in the rutile TiO_2 system than anatase TiO_2 under mercury lamp irradiation with Fe^{3+} ion as an acceptor (**Fig.3-1 upper**). In this experiment, the ratio of evolved oxygen molecules and iron(II) (Fe^{2+}) ion which was reduced product of Fe^{3+} was almost shown as 0.25 which was the stoichiometric ratio in ST-G2/Fe^{3+} system (**Fig. 3-1 lower**).

However, in spite of many discussion about the improvement of oxygen evolution reaction activity, the mechanism of oxygen evolution through multielectron transfer process, and the photoabsorption i.e. the first step of photocatalysis have been never focused so far. For example, photocatalytic oxygen evolution from water proceeds by four-positive hole in total. Taking into account that possible standard electrode potentials (SEPs) for oxidation of water to hydroxyl radical, hydrogen peroxide or O_2, the number of transferred electrons (n_{et}) is formally one, two or four [Bard 1985].

However, there seems to be no effective method to determine the number for any OE reactions, not limited to photocatalysis, except for electrolytic OE in which its electrode potential might suggest n_{et}, and it has been generally defined the oxygen evolution from water proceeds as the +1.23 V process. But, the SEPs are based on the thermodynamics. In this case, the activity of electron transfer in metal electrode is defined as a unity. Therefore, the number of electron exchanging between electrode and substance is always guaranteed. On the other hand, the activity of electron is not guaranteed in a photocatalyst particle because the charge carrier, i.e., the pair of excited electron-positive hole is produced by incident photon absorption. The electron exchanging between photocatalyst and substance must simultaneously occur, therefore, the photocatalytic reaction efficiency may depend on the irradiation light intensity. Although it has been rarely discussed about the correlation of thermodynamics and kinetics. The clarification of n_{et} in photocatalytic oxygen evolution is one of the important factor for designing high efficiency artificial photosynthesis system.

In this **chapter 3**, the light intensity-dependent kinetics of titanium(IV) oxide (titania)-photocatalyzed oxygen evolution was presented and show, for the first time in non-electrochemical multielectron transfer processes, n_{et} depending on the titania photocatalysts and reaction conditions. This fact suggests that multielectron transfer is digitally controlled by the number of positive hole, i.e. kinetics not only possible SEPs based on the

thermodynamics as a novel concept, and show the significant fourth-order dependence, i.e., "singularity" in chemical kinetics. In addition, the influence of particle-size of TiO_2 and electron acceptor in photocatalytic oxygen evolution were discussed based on the kinetic equation which derived from the kinetic reaction model. According to this analysis, it was clarified that "effective particle size" which was defined as the virtual particle-size of multielectron accumulation guaranteeing was the important factor to proceed the Multielectron transfer process.

3-2 Effect of Physical Property of TiO_2 and Electron Acceptor in Photocatalytic Oxygen Evolution

3-2-1 Rutile TiO_2 System

In this study, the light-intensity dependence of reaction rate in photocatalytic oxygen evolution from water using iron (III) (Fe^{3+}) or iodate (IO_3^-) ion as an electron acceptor was analyzed. **Fig. 3-2 (upper)** shows the light intensity dependence of oxygen evolution reaction rate for the several rutile titania samples system under NSL type UV-LED irradiation. In the case of IO_3^- system with MT-150A (Tayca, 13 nm, SR), relatively lower light intensity region than the threshold intensity (I_{thr} = 80 mW), the higher-order light-intensity dependence was observed and reproduced by assuming the second-order dependence with least-square method. On the other hand, in the higher intensity region than I_{thr}, the dependency was changed from second to first order. Furthermore, in Fe^{3+} system, the second to first order dependence was also observed, however, the I_{thr} (= 190 mW) and overall reaction rate had become higher than IO_3^- system.

Moreover, the influence of photocatalyst particle-size for the light-intensity dependence was discussed using ST-G2 (Showa Denko Ceramics, 350 nm, LR) and calcined MT-150A at 973 K (SR973) in both electron acceptor system. In SR973 system, the threshold intensity and reaction rate of oxygen evolution was decreasing and increasing than natural sample's system, respectively. In contrast, there were no higher-order dependence observation and only first-order dependence was shown in LR system. The slope of double-logarithm plot which composed a light intensity and reaction rate, i.e., the reaction order of light intensity was suggested that the changing of order in SR and SR973 system (**Fig. 3-2 middle and lower**). The reaction rate in higher intensity region of larger particles, the proposal reaction rate were gradually decreased. It was suggested the diffusion limited process

These facts which were the second-order dependence in lower than threshold intensity on IO_3- and Fe^{3+} system, respectively, were suggested due to the multielectron

reaction in photocatalytic oxygen evolution from water. In general, photocatalytic oxygen evolution from water have considered that water oxidation through four positive hole reaction described below.

$$2H_2O + 4h^+ \rightarrow O_2 + 4H^+ (+ 1.23\ V) \quad (21)$$

According to the second-order dependence in the SR and SR973 system, it seemed that the two-electron transfer process proceeded in oxygen evolution from water through hydrogen peroxide production.

$$2H_2O + 2h^+ \rightarrow H_2O_2 + 2H^+ \quad (+ 1.77\ V). \quad (22)$$

In this study, the position of valance band top on TiO_2 photocatalyst is deep enough to drive the two-electron transfer process. When the four-hole accumulation in one photocatalyst particle is difficult in the low light-intensity region for TiO_2 system, two electron transfer reaction can proceed by two-accumulated positive hole in one particle. Although two-electron reaction proceeding, H_2O_2 was not detected in supernatant of sample solution using titanium sulfate. This fact was suggested that the lifetime of H_2O_2 produced by two–electron transfer process was shorter and H_2O_2 was immediately consumed by another positive holes to produce O_2 molecules. These findings were presumed that overall reaction rate were controlled by the reaction rate of the H_2O_2 production through two-electron transfer process. Moreover, the later oxidation step i.e., from H_2O_2 to O_2 might be faster and there were no influence for overall reaction rate.

The differences of reaction rate and threshold intensity depending on the kind of electron acceptors were indicated due to the ability of electron transferring to electron acceptor, and the detail of the kinetic effects were described in **Section 3-6**.

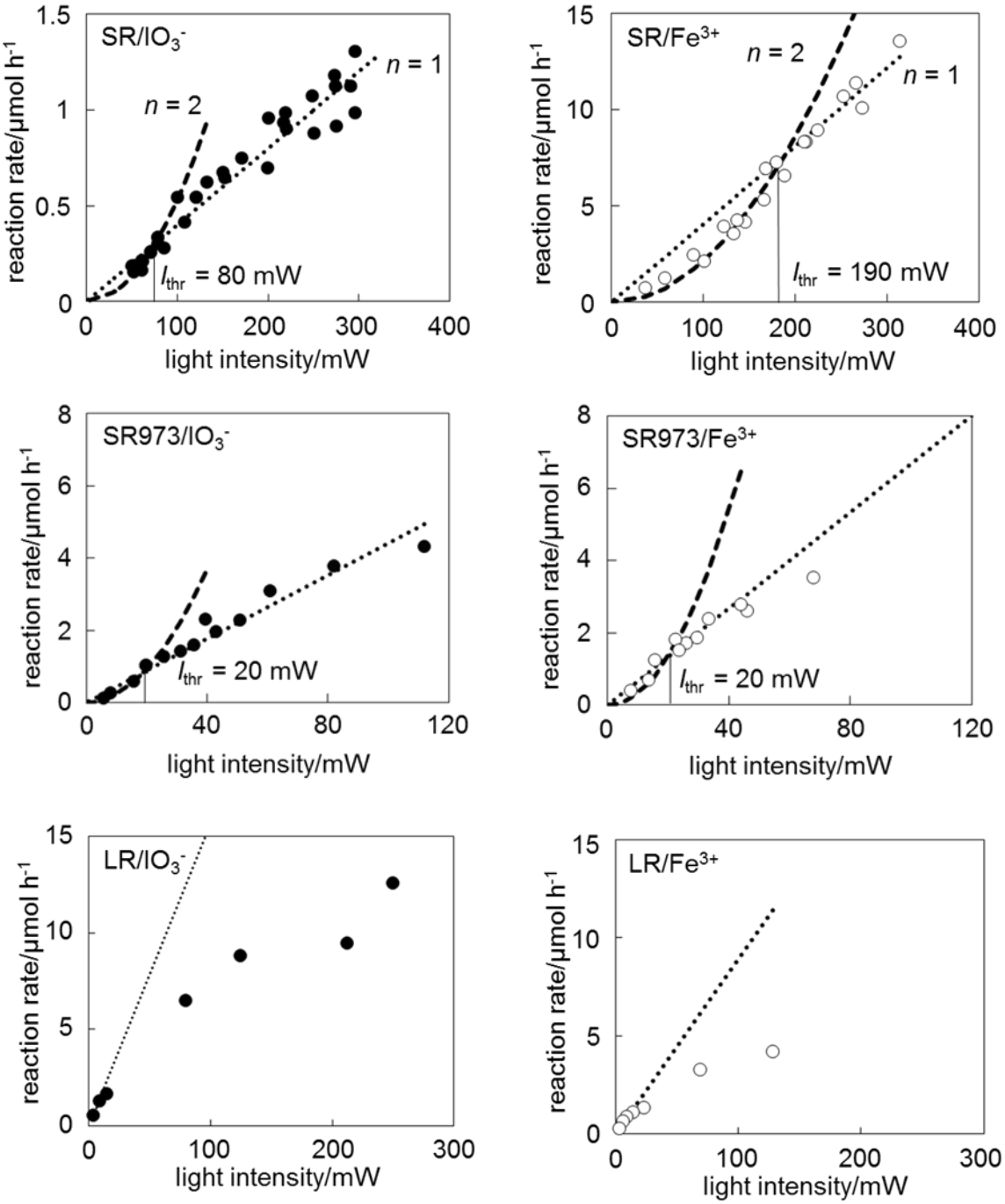

Fig.3-2 Light-intensity dependence of reaction rate of oxygen evolution using rutile TiO_2 in the presence of electron acceptor (IO_3^-, Fe^{3+})

3-2-2 Anatase TiO_2 System

It have been considered that anatase TiO_2 have negligible activity for photocatalytic oxygen evolution from water under ordinary light source such as high pressure mercury lamp or xenon lamp [Ohno 2001, Prieto 2009, Ohtani 2010, Maeda 2014]. In this thesis, the light intensity dependence of ST-01(Ishihara Sangyo, 4 nm, SA) and Fluka (170 nm, LA) system with both type of electron acceptors were measured under NSL type UV-LED irradiation in order to discuss about the influence of the crystallinity of TiO_2 (**Fig. 3-3**). According to the LA system, there were no higher-order dependence observation, and first-order which was the same tendency of LR system appeared. On the other hand, the second-order dependence was observed in the lower region than each threshold intensity in both electron acceptor as with SR and SR973 system, however, it was interestingly that the higher-order which could be approximated by fourth-order dependence was observed under intense light irradiation condition (>270 mW) in SA/IO_3^- system. It was suggested that the fourth-order dependence in SA/IO_3^- system might be due to the four-electron transfer process which was lower SEP than two-electron transfer process. These facts seem that the mechanism of multielectron transfer processes depending on the irradiation intensity.

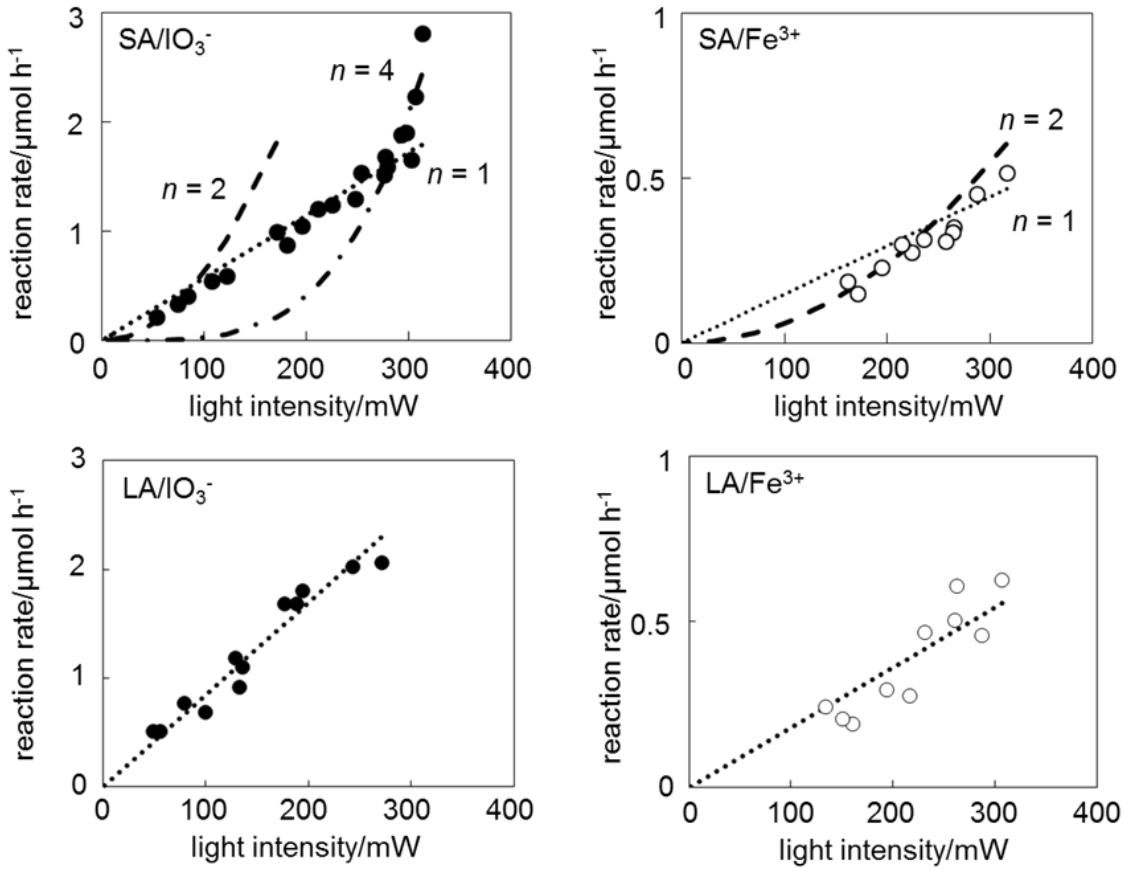

Fig.3-3 Light-intensity dependence of reaction rate of oxygen evolution using Anatase TiO_2 in the presence of electron acceptor (IO_3^-, Fe^{3+})

3-3 Influence of Photon Density in Photocatalytic Oxygen Evolution under Focused/Unfocused UV-LED Irradiation

As described above, the fourth-order dependence was observed in SA/IO_3^- system under NSL type UV-LED (the focused light) irradiation. According to this fact, it was assumed the light focusing might be influenced to the higher order dependence, i.e., second or fourth-order. Therefore, the unfocused type UV-LED (HMP type) was used for the analysis of light-intensity dependence in SA/IO_3^- system to consider the influence of light focusing property in photocatalytic oxygen evolution.

The comparison of light intensity dependence of reaction rate under NSL and HMP type UV-LED irradiation was shown as **Fig.3-4**. In the case of HMP type irradiation, the second-order dependence was shown in the same light intensity range of NSL type irradiation. However, there was no fourth-order dependence observation under higher intensity region in spite of same or higher intensity of the fourth-order range in NSL type irradiation. When the irradiation light intensity adjusted, the distance was changed between the light source and quartz cell for NSL type. On the other hand, in the case of HMP type, only source power adjusted without LED-Cell distance changing. Therefore, these difference of light-intensity dependence (fourth-order dependence) was indicated due to the incident photon density and affecting to the overall reaction mechanism and/or rate of multielectron reaction.

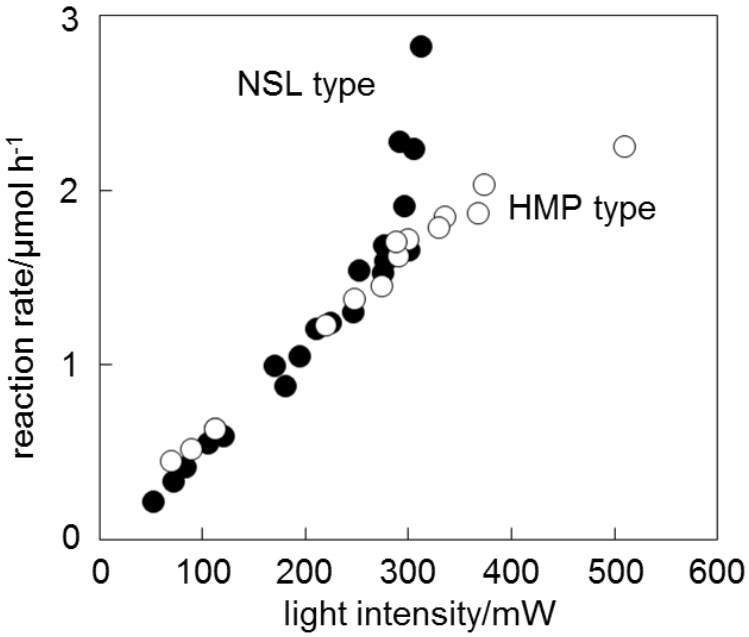

Fig.3-4 Light-intensity dependence of reaction rate of oxygen evolution under different type UV-LEDs in SA/IO_3^- system

In order to correct the focusing properties for each UV-LED light source, the light intensity distribution in 1 cm^2 area and the total power intensity was calculated and derived. The detail of light intensity distribution measurement and derivation of total irradiation light intensity using a light-intensity distribution was already described in **chapter 2**.

Fig.3-5 showed the irradiation light intensity distribution and the total of the photon density for each of NSL and HMP type UV-LED. The effective irradiation area (A_{95}) was derived from the 95% power passing which calculated from the total incident light intensity in a 1 cm^2 aperture. The total light intensity (I_L) wes evaluated from eq. (19).

Fig. 3-6 was shown the light intensity (corrected) dependence of reaction rate anatase and rutile TiO_2 in the presence of IO_3^- system. The large size of anatase and rutile, i.e., LA and LR were observed the first-order dependence. In the case of SR and SR973 system were still shown the changing from second to first-order dependence, and SA also observed the second to first, and fourth-order dependence. The lower intensity region of SA system, the light intensity dependence (LID) under HMP and NSL type irradiation gave almost the same plots despite of different focus properties. It was indicated that the

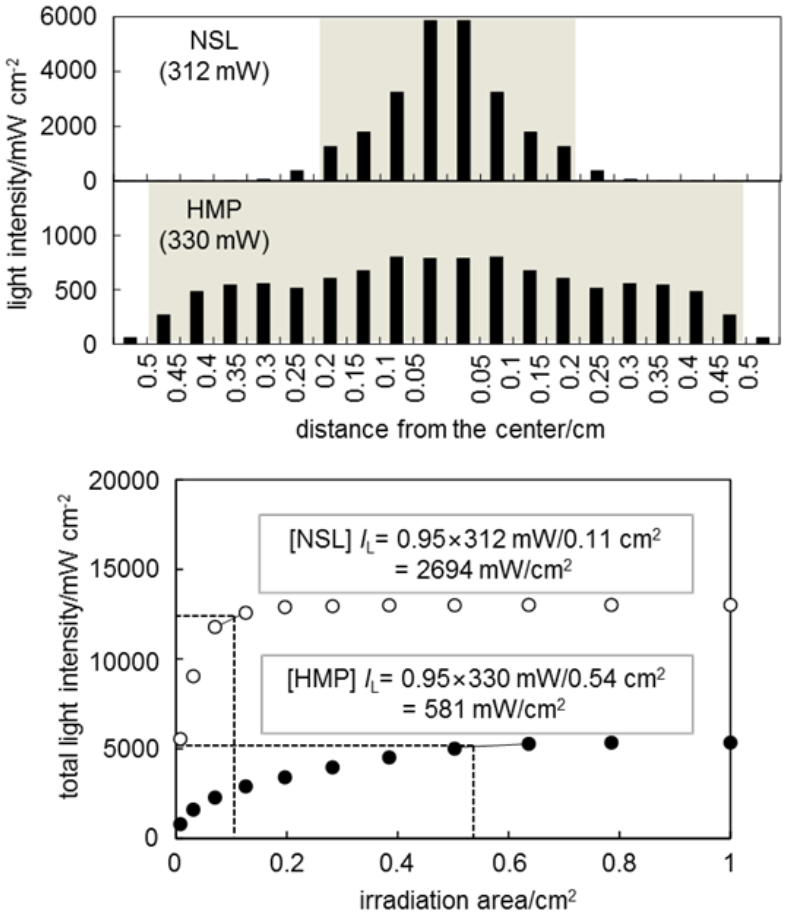

Fig.3-5 (upper) Examples of light-intensity distribution of NSL and HMP UV-LEDs. Colored areas indicate effective irradiation area (A_{95}). (lower) Calculation of A_{95} and I_L from light-intensity distributions.

inhomogeneity correction of light intensity was reasonable. In other words, the reaction rate of photocatalytic oxygen evolution per unit area were governed by I_L, and even if total power of irradiated light is the same, different values of I_L induce different overall reaction rates in the higher-order dependence region.

As shown in **Fig. 3-7**, the double-logarithm plots of IO_3^- system indicated. The approximated curve were roughly reproduced by the function (polynomial equation) curve fitting using Igor software (Wavemetrics Inc.). The reaction order was calculated from the changing from the approximated curve slope. In the case of SR and SR973 system the reaction order were changed from second to first, in contrast, SA system indicated the order also changing from second to first, and then almost fourth-order. The order in LR and LA were almost first as the constant or gradually decreasing due to the diffusion limited process of subsequent in aqueous.

On the other hand, **Fig. 3-8 and 3-9** were shown the light-intensity dependence and double-logarithm plot in Fe^{3+} system. As also described above, I_L dependency was still maintained regardless of inhomogeneity correction. The reaction order were changing from second to first in SR and SR973 system and the large particle was almost unity. These facts supported the higher-order dependence due to the multielectron water oxidation reaction, and suggested the reaction mechanism of photocatalytic multielectron transfer reaction and the rate was depending on the I_L intensity i.e. the kinetics.

According to the above mentions, it was considered the reaction mechanism correlated between the kinetics and thermodynamics. It has been generally considered that photocatalytic oxygen evolution through water oxidation is defined as the four positive hole reaction based on +1.23 V as SEP. In the lower I_L range in small TiO_2 system, the second-order dependence indicates due to the two-electron transfer process ($2H_2O + 2h^+ \rightarrow H_2O_2 + H_2$ (+1.77 eV)). In lower I_L condition, it is hardly accumulated the four-positive holes in one photocatalyst particle at the same time during the lifetime of one positive hole produced by photon absorption due to low number of incident photon. In this study, TiO_2 using as the photocatalyst can proceed the two-electron transfer process (+1.76 V) according to the position of valence band top (+3.0 eV or +3.2 eV, rutile and anatase, respectively). Therefore, in the condition which two positive hole guaranteed in one photocatalyst particle, photocatalytic oxygen evolution proceeded through the oxidation of hydrogen peroxide produced by the two-electron transfer process. In the middle I_L region, the reaction order was changed from second to first. The first-order dependence was suggested the reaction efficiency become constant because two accumulated positive hole might be always guaranteed, therefore, two-electron transfer process proceeded through H_2O_2 production in the second to first-order intensity region. This assumption can follow the change of LID-order. According to double-logarithm plots of SR, SA, and SR873 in **Fig. 3-7, 3-9**, these LID-orders were gradually changed from second to first-order. When I_L increasing, the

probability of two positive hole production is also guradually increasing, and then, the two photon absorption is always guaranteed and the probability become constant. Therefore, the LID order gradually decreased to first-order.

On the other hand, in the higher I_L condition, it is possible to pool the four-positive hole in one particle at the same time, since the four-electron process defined as +1.23 V which has lower SEP than the two-electron transfer occur preferably. It is reasonable to expect four-positive hole accumulation in one particle under high I_L light irradiation and observe the fourth-order dependence, i.e., singularity.

Based on above discussion, it was indicated that the mechanism and reaction rate of multielectron reaction were depending on the kinetics and thermodynamics, i.e. light intensity and SEPs. In photocatalysis, the number of charge carrier were not guaranteed because the activity was not unity, thus, incident light intensity affected to the number of carrier in photocatalyst particle. Although, it was generally discussed the mechanism of photocatalysis especially multielectron transfer process based on the SEP based on thermodynamics. Previously, kinetics of chemical reaction included photocatalysis have been defined as the analogue function according to the concentration of substances. The singularity fourth-order dependence suggests the reaction mechanism changing from two-electron transfer to four-electron transfer process. This facts indicate the kinetics of photocatalytic multielectron transfer process are controlled digitally by the number of photon absorption in one photocatalyst particle.

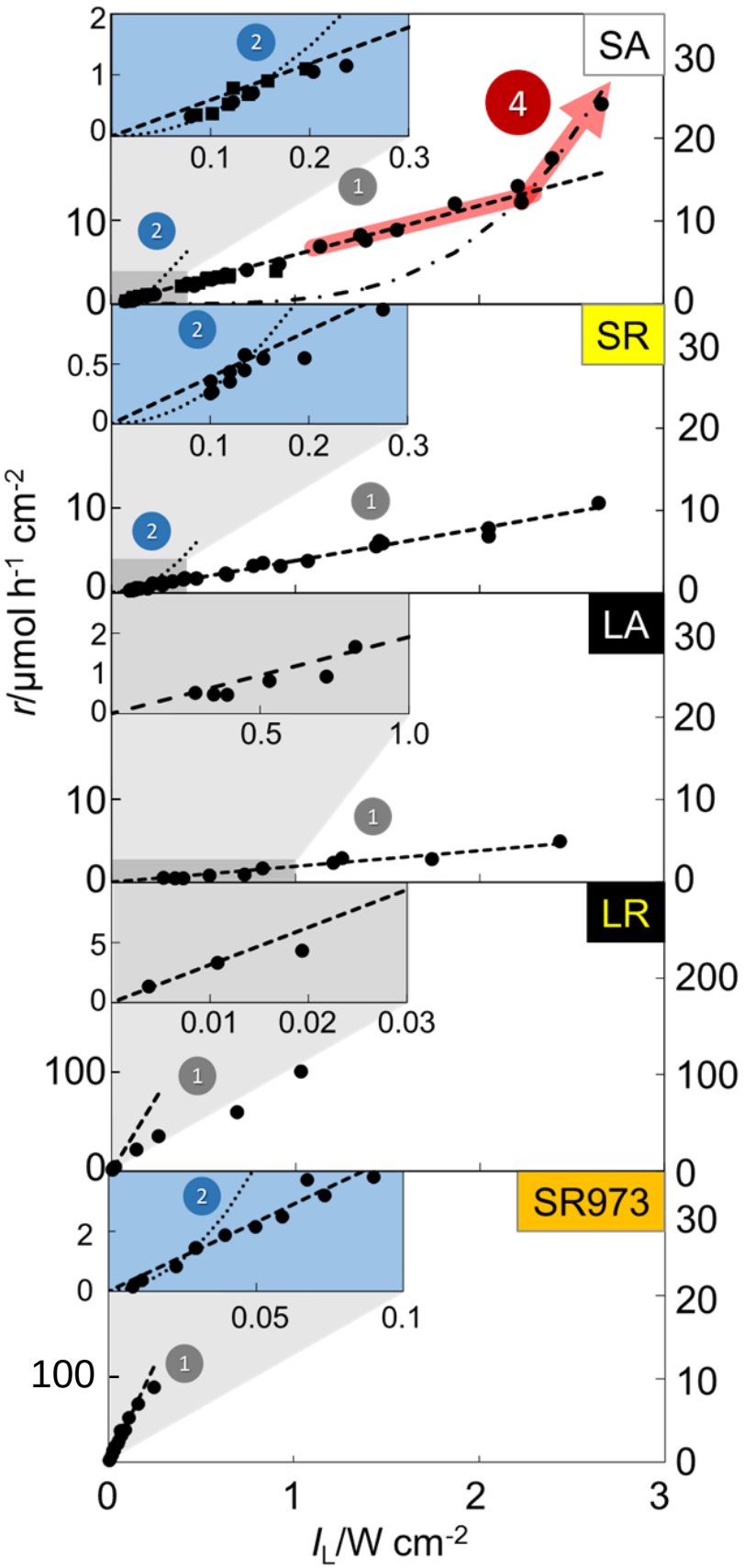

Fig. 3-6 Corrected light-intensity dependence of reaction rate for each titania samples in the presence of IO_3^- as an electron acceptor.

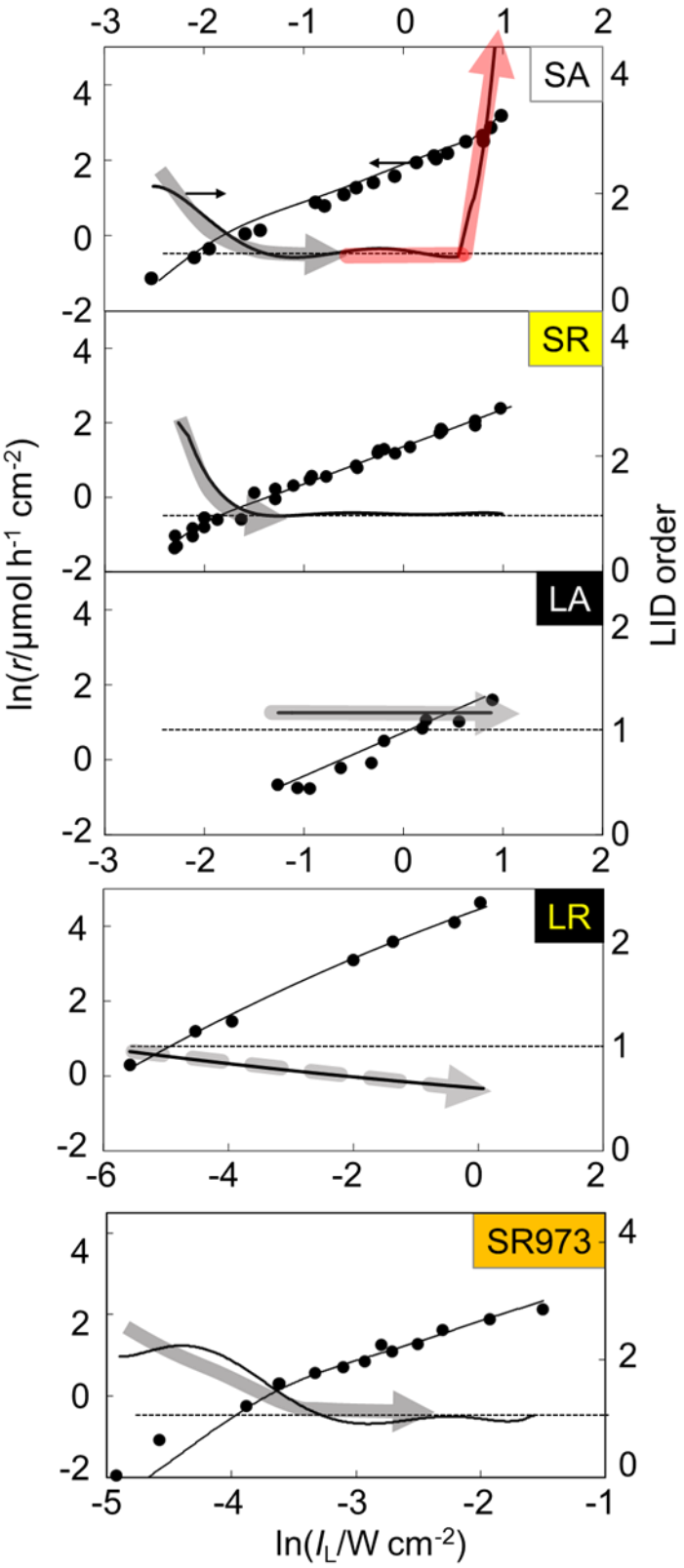

Fig. 3-7 Double-logarithm plot of corrected light-intensity dependence of reaction rate for each titania samples in the presence of IO_3^- as an electron acceptor.

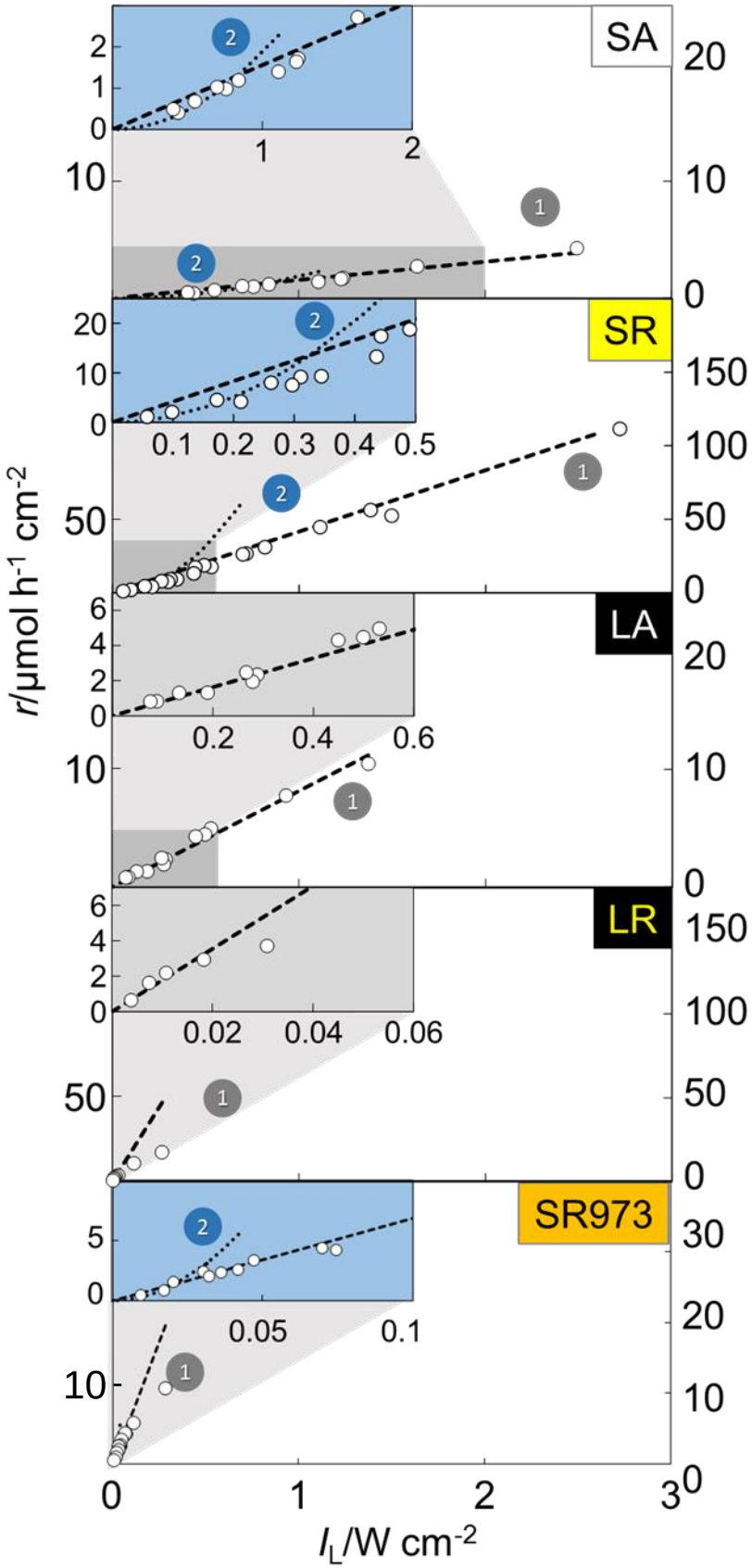

Fig. 3-8 Corrected light-intensity dependence of reaction rate for each titania samples in the presence of Fe^{3+} as an electron acceptor.

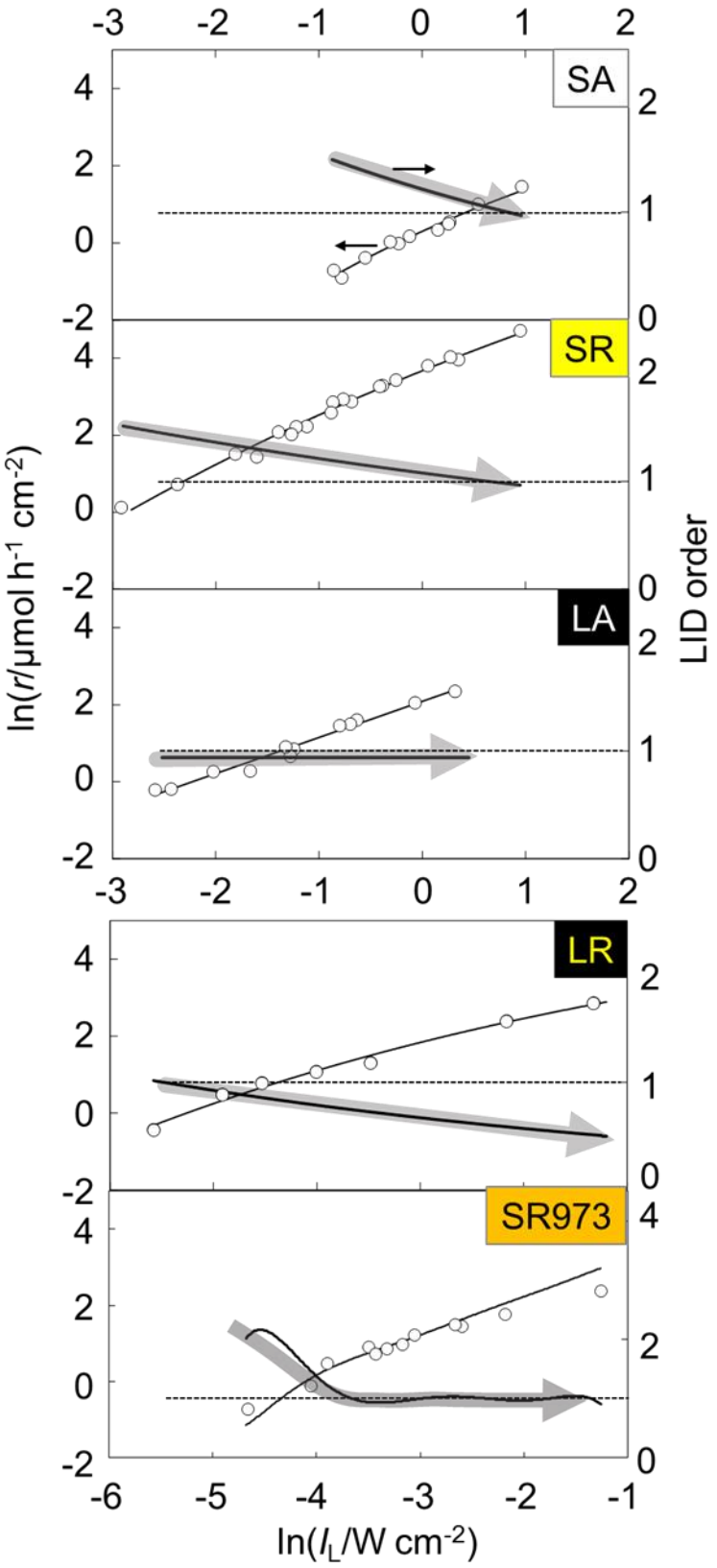

Fig. 3-9 Double-logarithm plot of corrected light-intensity dependence of reaction rate for each titania samples in the presence of Fe^{3+} as an electron acceptor.

3-4 Kinetic Model of Two-electron Transfer Model in Photocatalytic Oxygen Evolution

As discussed above, the light intensity dependence of photocatalytic oxygen evolution reaction rate was analyzed. In the case of small rutile and anatase system, the observation of second to first order light intensity dependence was suggested due to oxygen evolution through the two-electron transfer process produced hydrogen peroxide. As **Fig. 3-6** and **3-8** shown, the threshold light intensity of second to first order dependence and the reaction rate were depending on the kind of electron acceptor and photocatalyst particle size. In order to analyze these influences, the two-electron reaction model which was defined by some kinetic parameters was constructed to derive the kinetic equations. **Scheme 1** shows the two-electron reaction model in photocatalytic oxygen evolution. According to the model, a photocatalyst particle (TiO_2) absorbs light to create an excited electron (e^-)-positive hole (h^+) pair at first. In this case, the possibility of multiple-photon absorption in one particle was neglected. The pair is captured by an electron acceptor (EA) ion (Fe^{3+} or IO_3^-) on the surface of photocatalyst to leave h^+ accompanied by a one-electron reduced EA([h^+-EA^-]) (e.g., iron(II) ion when Fe^{3+} is used as an electron acceptor) ([h^+]) or disappears by its mutual recombination process. In the first photoabsorption step, the rate of [h^+] liberation is expressed by the product of I_L (/W (=J s^{-1}) cm^{-2}), photoabsorption efficiency (ψ/mol J^{-1}) and quantum efficiency of e^- capture (φ), in which ψ and φ depend on only the composition of a photocatalyst and EA/ photocatalyst-particle properties, respectively. The consumption of [h^+] are assumed for two paths: one is back electron transfer to regenerate an electron acceptor ion with the lifetime τ_1, and the other is the second photon absorption of [h^+] to create two h^+-bearing particles ([h^+h^+]) with the rate of $I_L\psi_2\varphi$. It is presuming that the quantum efficiency for second positive hole (electron) creation is assumed to be the same as φ for convenience, and ψ_2 is smaller than ψ since this second-photon absorption is limited only to [h^+], not all photocatalyst particles. It is similar to [h^+] case, the two paths are also assumed for [h^+h^+]: back (two) electron transfer to the original non-charged particle [TiO_2] with lifetime τ_2 (Even when one-electron back transfer from [h^+h^+] to [h^+-EA^-] is assumed, the derived overall rate equation is identical to [Eq. (30)], since the employed assumption, $k >> 1/\tau_2$, leads to neglection of the back electron-transfer process from [h^+h^+] and the rate of hydrogen-peroxide liberation is the same as that of [h^+h^+] liberation.) and reaction with two water molecules to release hydrogen peroxide (H_2O_2) with a rate constant *k*. In this case, the reaction rate of H_2O_2 to O_2 is assumed not to affect for overall reaction rate, since H_2O_2 is stable and has more cathodic (oxidation) SEP ($O_2 + 2e^- + 2H^+ = H_2O_2$: 0.70 V vs SHE) than that of water ($H_2O_2 + 2e^- + 2H^+ = 2H_2O$: 1.76 V vs SHE). Therefore, the liberation rate of the final oxidation product, O_2, is the same as the H_2O_2 production rate.

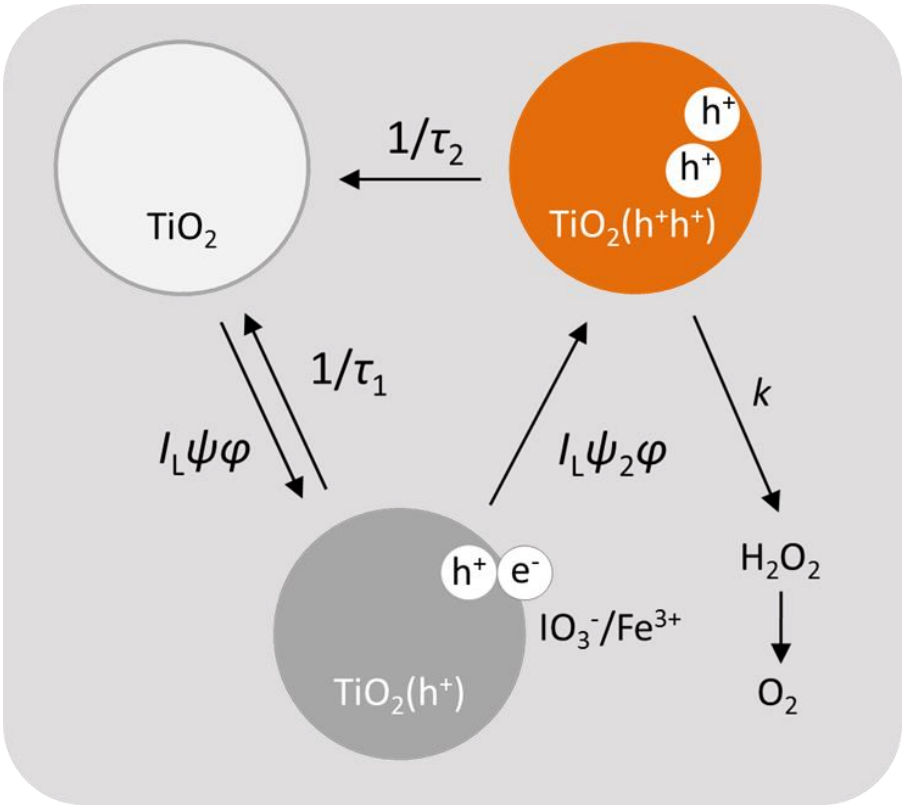

Scheme 1 two-electron transfer reaction model of photocatalytic oxygen evolution

3-4-1 Derivation of Kinetic Equation in Two-electron Transfer Process

According to the two-electron transfer model (**Scheme 1**), the steady-state approximation was applied for hole-bearing TiO_2 species to derive the kinetic equation. In photocalalysis, it is difficult to clarify the actual reaction mechanism completely because of the reaction proceeding through complicated elementally processes. Therefore the steady-state approximation have been ordinary applied to excited species i.e. charge carriers for consideration of the mechanism [Freischauer 1972, Murakami 2007]. In this case, the derived kinetic equations are as shown below. The reaction rate of each activation and deactivation step through photoabsorption can indicate as

$$TiO_2 + h\nu \rightarrow TiO_2(h^+) \qquad r = I_L\psi\varphi \quad (21)$$

$$TiO_2(h^+) \rightarrow TiO_2 \qquad r = 1/\tau_1[TiO_2(h^+)] \quad (22)$$

$$TiO_2(h^+) + h\nu \rightarrow TiO_2(h^+h^+) \qquad r = I_L\psi_2\varphi[TiO_2(h+)] \quad (23)$$

$$TiO_2(h^+h^+) \rightarrow TiO_2 \qquad r = 1/\tau_2[TiO_2(h^+h+)] \quad (24)$$

$$TiO_2(h^+h^+) \rightarrow TiO_2 + H_2O_2 \qquad r = k[TiO_2(h^+h^+)] . \quad (25)$$

And then, the steady state approximation is applied to the concentration of hole bearing TiO_2, i.e., $[TiO_2(h^+)]$ and $[TiO_2(h^+h^+)]$ as shown below.

$$[TiO_2(h^+)] = I_L\psi\varphi/(1/\tau_1 + I_L\psi_2\varphi) \quad (26)$$

$$[TiO_2(h^+h^+)] = I_L\psi_2\varphi[TiO_2(h^+)]/(1/\tau_2 + k) \quad (27)$$

According to the above assumption ($k >> 1/\tau_2$), the overall kinetic equation is expressed as

$$r = k[TiO_2(h^+h^+)] = \frac{I_L^2\psi\psi_2\varphi^2}{(1/\tau_1) + I_L\psi_2\varphi} . \quad (28)$$

At the low and high limits of I_L, the rate equation is simplified as in [Eq. (29)] and [Eq. (30)], and the LIDs of the overall OE rate are second and first order, respectively, reproducing the observed LIDs for the SR sample.

$$r_{\mathrm{low}} = I_{\mathrm{L}}^2 \psi \psi_2 \varphi^2 \tau_1 \quad (29)$$

$$r_{\mathrm{high}} = I_{\mathrm{L}} \psi \varphi \quad (30)$$

This kinetic model means that accumulation of two positive holes is required and the probability of liberation of [h^+h^+] in the lower I_L range is proportional to the square of I_L, while in the higher I_L range, the required two-photon absorption is guaranteed and the rate is simply proportional to I_L, therefore, the rate is not depending on the lifetime of positive hole (τ_1, τ_2). And then, the virtual threshold I_L (I_{thr}) at which an LID order is changed from two to one is obtained by assuming $r_{low} = r_{high}$ as

$$I_{\mathrm{thr}} = \frac{1}{\psi_2 \varphi \tau_1}. \quad (31)$$

According to the **Scheme 1** and derived equation, the dependency changing i.e., LID-order gradually changing from second to first order was reproduced, based on the two-electron transfer process. The equation of first-order rate and I_{thr} were used for the kinetic analysis described in **section 3-7**.

3-4-2 Kinetic Model of Four-electron Transfer Process

In the case of small anatase with IO_3^- system, the second to first order changing in the lower I_L region, and then, the dependence were changed from first to fourth order under higher I_L region. As described above, these difference dependency changing is suggested due to the two-electron ($H_2O_2 + 2e^- + 2H^+ = 2H_2O$: 1.76 V vs SHE) and four-electron ($O_2 + 4e^- + 4H^+ = H_2O$: 1.23 V vs SHE) transfer water oxidation process, respectively. **Scheme 2** is the four-electron transfer reaction model including the two-electron transfer reaction. In the first photoabsorption step shown in the right side half, two-electron reduction mechanism is the same as that in **Scheme 1**. In the **Scheme 2**, further accumulation of positive holes was assumed to produce [$TiO_2(3h^+)$], which absorbs a photon in a similar way with $I_L\psi_4\varphi$ to produce a four positive hole-bearing particle [$4h^+$]. Finally, [$4h^+$] reacts with two water molecules to produce oxygen with a rate constant k_4. In this scheme, the recombination step were assumed that each positive hole bearing particle ($TiO_2(h^+)$, $TiO_2(h^+h^+)$, $TiO_2(3h^+)$, $TiO_2(4h^+)$) directly deactivated to neutral TiO_2.

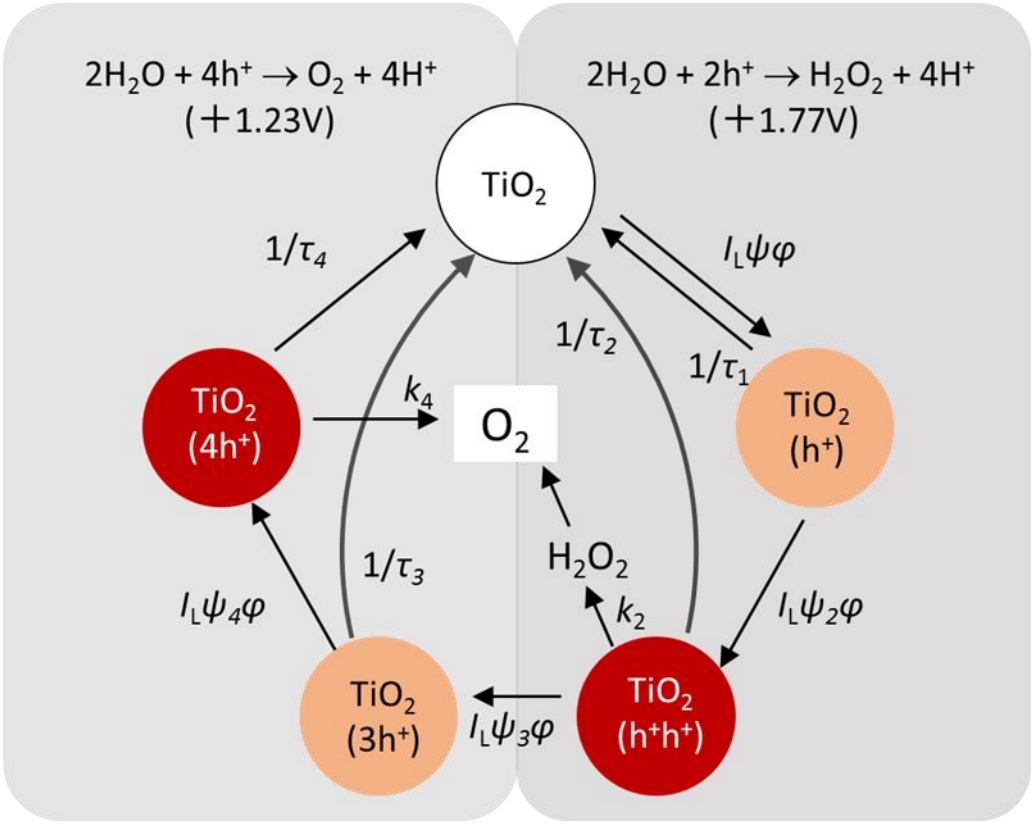

Scheme 2 Four-electron transfer reaction model of photocatalytic oxygen evolution

3-4-3 Derivation of Kinetic Equation in Four-electron Transfer Process

According to the **Scheme 2**, kinetic equations can reproduce the light-intensity dependency of four-electron transfer process. As shown below, each activation with photoabsorption and deactivation step defined to derive the kinetic equation.

The right side of **scheme 2** is the same of two-electron transfer process, therefore the photoabsorption step can indicate as the same.

$TiO_2 + h\nu \rightarrow TiO_2(h^+)$ $\quad r = I_L\psi\varphi$ (32)

$TiO_2(h^+) \rightarrow TiO_2$ $\quad r = 1/\tau_1[TiO_2(h^+)]$ (33)

$TiO_2(h^+) + h\nu \rightarrow TiO_2(h^+h^+)$ $\quad r = I_L\psi_2\varphi[TiO_2(h+)]$ (34)

$TiO_2(h^+h^+) \rightarrow TiO_2$ $\quad r = 1/\tau_2[TiO_2(h^+h+)]$ (35)

and the further photoabsorption step are shown below.

$TiO_2(h^+h+) + h\nu \rightarrow TiO_2(3h^+)$ $\quad r = I_L\psi_3\varphi[TiO_2(h^+h^+)]$ (36)

$TiO_2(3h^+) \rightarrow TiO_2$ $\quad r = 1/\tau_3[TiO_2(3h^+)]$ (37)

$TiO_2(3h^+) + h\nu \rightarrow TiO_2(4h^+)$ $\quad r = I_L\psi_4\varphi[TiO_2(3h^+)]$ (38)

$TiO_2(4h^+) \rightarrow TiO_2$ $\quad r = 1/\tau_4[TiO_2(4h^+)]$ (39)

$TiO_2(4h^+) \rightarrow TiO_2 + O_2$ $\quad r = k_4[TiO_2(4h+)]$ (40)

The steady state approximation is also applied for the concentration of each hole bearing TiO_2 particle to derive the each concentration as

$$[TiO_2(h^+)] = I_L\psi\varphi/(1/\tau_1 + I_L\psi_2\varphi) \quad (41)$$

$$[TiO_2(h^+h^+)] = I_L\psi_2\varphi[TiO_2(h^+)]/(1/\tau_2 + I_L\psi_3\varphi) \quad (42)$$

$$[TiO_2(3h^+)] = I_L\psi_3\varphi[TiO_2(h^+h^+)]/(1/\tau_3 + I_L\psi_4\varphi) \quad (43)$$

$$[\mathrm{TiO_2(4h^+)}] = I_{\mathrm{L}}\psi_4\varphi[\mathrm{TiO_2(3h^+)}]/(1/\tau_4 + k). \quad (44)$$

The overall reaction rate in four-electron transfer process is derived as

$$r = k_4[Ti\mathrm{O_2(4h^+)}] = \frac{k_4 I_{\mathrm{L}}^4 \psi\psi_2\psi_3\psi_4\varphi^4}{(I_L\psi_2\varphi + 1/\tau_1)(I_L\psi_3\varphi + 1/\tau_2)(I_L\psi_4\varphi + 1/\tau_3)(1/\tau_4 + k_4)}. \quad (45)$$

At the low and high limits of I_{L}, the rate equation is simplified as in [Eq. (46)] and [Eq. (47)], and the LIDs of overall OE rate are fourth and first order, respectively.

$$r_{\mathrm{low}} = \frac{k_4 I_{\mathrm{L}}^4 \psi\psi_2\psi_3\psi_4\varphi^4\tau_1\tau_2\tau_3}{k_4 + 1/\tau_4} \quad (46)$$

$$r_{high} = \frac{k_4 I_L \psi\varphi}{k_4 + 1/\tau_4} \quad (47)$$

According to the simplified equation, it is indicated the light intensity dependences change from fourth to first-order. If the four positive holes are sufficiently produced by light irradiation, the probability and reaction efficiency of multielectron transfer become constant, and then, the higher-order dependence change to first order as similar as the two-electron transfer process.

As derived the kinetic equations on two-electron and four-electron process indicate the digitally controlling of multielectron process. The two-electron and four-electron transfer models (**Scheme 1 and Scheme 2**) can derive the kinetics of second to first-order, or fourth-order dependence, but, first to fourth, i.e., two-electron to four-electron process can't reproduce directly from these kinetic models because the number of electron transfer is different, therefore, the first to fourth-order changing due to digitally controlled kinetics depending on the number of hole accumulation.

3-5 Oxygen Isotope Experiments of Photocatalytic Oxygen Evolution

According to the light intensity dependence of photocatalytic reaction rate of oxygen evolution in the presence of electron acceptor, there were the second and fourth order dependence observation suggesting due to the two-electron and four-electron transfer process, respectively. In this study, oxygen-isotope experiments using heavy oxygen-rich water ($H_2{}^{18}O$) was discussed for considering the atomic source of produced oxygen. The experiment condition of isotope experiment was already discribed above.

Oxygen-isotope experiments were performed using large rutile(ST-G2) or small anatase (ST-01) sample suspended in a 75/25 mixture of Milli-Q water ($H_2{}^{16}O$) and isotope-labeled water ($H_2{}^{18}O$; ≧99.8%, Taiyo Nippon Sanso) water containing IO_3^- or iron(III) (Fe^{3+}) ions as EA systems under NSL UV-LED irradiation (> 2.5 W cm^{-2}). Liberated oxygen was analyzed by a gas chromatograph-mass spectrometer (Shimadzu GC-17A/GCMS-QP5050A). The atomic content of ^{18}O (^{18}O content) in liberated oxygen was calculated with the following equation; ^{18}O content = $1/(1 + (I_p(^{16}O^{18}O) / I_p(^{18}O_2))$, where $I_p(^{16}O^{18}O)$ and $I_p(^{18}O_2)$ are relative intensity of $^{16}O^{18}O$ (m/e = 34) and $^{18}O_2$ (m/e = 36) peak intensities on the assumption that $^{16}O_2$ was contaminated by air and $^{16}O_2$-peak intensity could not be used for calculation. The theoretical ^{18}O content was calculated by assuming the purity of the $H_2{}^{18}O$ to be 99.8% to be 0.245.

As shown below indicated that the liberated oxygen was originated from water, not iodate (IO_3^-), even when IO_3^- was used as an electron accepter. Furthermore, there was an almost stoichiometric molar ratio of liberated O_2 to consumed EAs according to the equations as

$$Fe^{3+} + e^- = Fe^{2+}, \quad (17)$$

$$IO_3^- + 3H_2O + 6e^- = 6OH^- + I^- \quad (18)$$

$$O_2 + 4H^+ + 4e^- = 2H_2O \quad (1.23\ V) \quad (8)$$

These facts also suggest that the process of OE, not electron transfer from a photocatalyst to EAs, accounts for the observed unconventional LIDs.

In two repeated experiments using ST-01 and IO_3^- as a photocatalyst and an EA, respectively, observed ^{18}O content was almost equal to the theoretical value during the course of photocatalytic reaction (The reason for slightly lower value at 30-min irradiation in the first experiment is unknown at present, but some surface hydroxyls or adsorbed water might participate). When LR and Fe^{3+} were used as a photocatalyst and an EA, respectively, the observed ^{18}O content was also close to the theoretical value. Therefore, it is concluded

that the origin of liberated oxygen is water, not the other oxygen-containing compounds such as IO_3^- ions. The exception was LR/IO_3^- case; at first, the ^{18}O content was slightly lower than 0.245, decreased gradually with photoirradiation, and seemed be saturated at the longer irradiation time. Extrapolation of these plots to time zero could be close to the theoretical value, i.e., it can be presumed that ^{18}O content at the commencement of photoirradiation was equal to 0.245 as was observed in the other reaction systems, but the content was decreased by prolonged photoirradiation. A possible explanation is photoinduced oxygen isotope exchange (POIE) on the surface of large rutile [Sato 1984, Sato 1987, Mikhaylov 2012]. The serious mechanism of POIE on the surface of TiO_2 in alkaline conditions is not clarified the detail, but the effect of pH and/or the active energy of POIE depending on the crystallinity might be influenced.

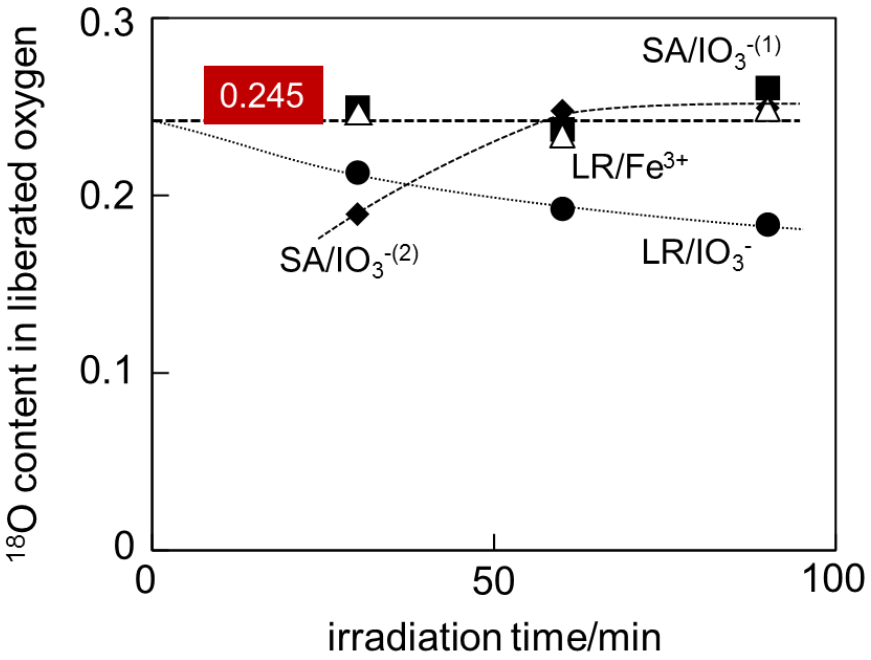

Fig. 3-8 ^{18}O content in oxygen liberated from the suspensions of SA and LR titania samples with IO_3^- and Fe^{3+} ions as an EA (Closed circle, triangle, closed square, and rhombus correspond to LR/IO_3^-, LR/Fe^{3+}, SA/IO_3^-(first time), SA/IO_3^-(second time), respectively.)

3-6 Kinetic Analysis of the Particle-size and Electron Acceptor Effects in Photocatalysis Oxygen Evolution

3-6-1 About the Kinetic Analysis

As already mentioned above, the second to first order dependence changing was observed especially in the case of small particle-size anatase and rutile TiO_2 system with IO_3^- and Fe^{3+} as an electron acceptor. These dependency could be reproduced from the kinetic equations derived from **Scheme 1**. According to the kinetic parameters in the equations, the influence of particle-size of TiO_2 and electron acceptor were discussed in the overall reaction rate and the threshold intensity (I_{thr}). The kinetic parameters were compared by the relative value which was MT-150A/IO_3^- system as the basis. The reaction rate of oxygen evolution was in the range of first-order dependence($I_L\psi\varphi$), and the I_{thr} was inverse of the intensity($\psi'\varphi\tau_1$).

3-6-2 Photocatalyst Particle-size Effect

Table 1 shows the influence of the particle size of TiO_2 for the reaction rate and I_{thr} using IO_3^- as an acceptor. The I_{thr} was decreased according to the particle-size increasing. The lower I_{thr} of large particle-size system was indicated due to increasing of photoabsorption efficiency of one positive hole bearing TiO_2 ($TiO_2(h^+)$) (ψ'). In the case of large particle, the number of absorbed photon is guaranteed in lower intensity because of the large size of cross-section, hence the probability of another photon absorption become higher during the lifetime of one-positive hole. Therefore, I_{thr} was decreasing mainly due to ψ' increasing depending on the particle-size. In this case, the particle-size which can guarantee the two-positive hole accumulation i.e. "effective particle-size" is not equal to the physical particle-size. The larger particle-size photocatalyst can absorb the number of multiple photon, and also, physical distance of each positive holes might be also increased, thus, the probability of multielectron transfer can decrease. Therefore, it is important to consider the "effective particle-size" of photocatalyst for designing in photocatalytic multielectron transfer process. On the other hand, the reaction rate was increasing with the particle-size. The photoabsorption efficiency (ψ) is defined as a constant for each TiO_2 sample, therefore efficiency of electron transfer (φ) might be changed due to affecting for multielectron reduction efficiency of IO_3^-. Furthermore, the influence of particle-size was also discussed in another photocatalyst system. In the case of large particle size strontium titanate ($SrTiO_3$, >100 nm, 5 μm) system, the second-order dependence was not observed. It is suggested that the particle-size effect of photocatalyst, not only for TiO_2 system, affect to the multielectron transfer process in photocatalysis.

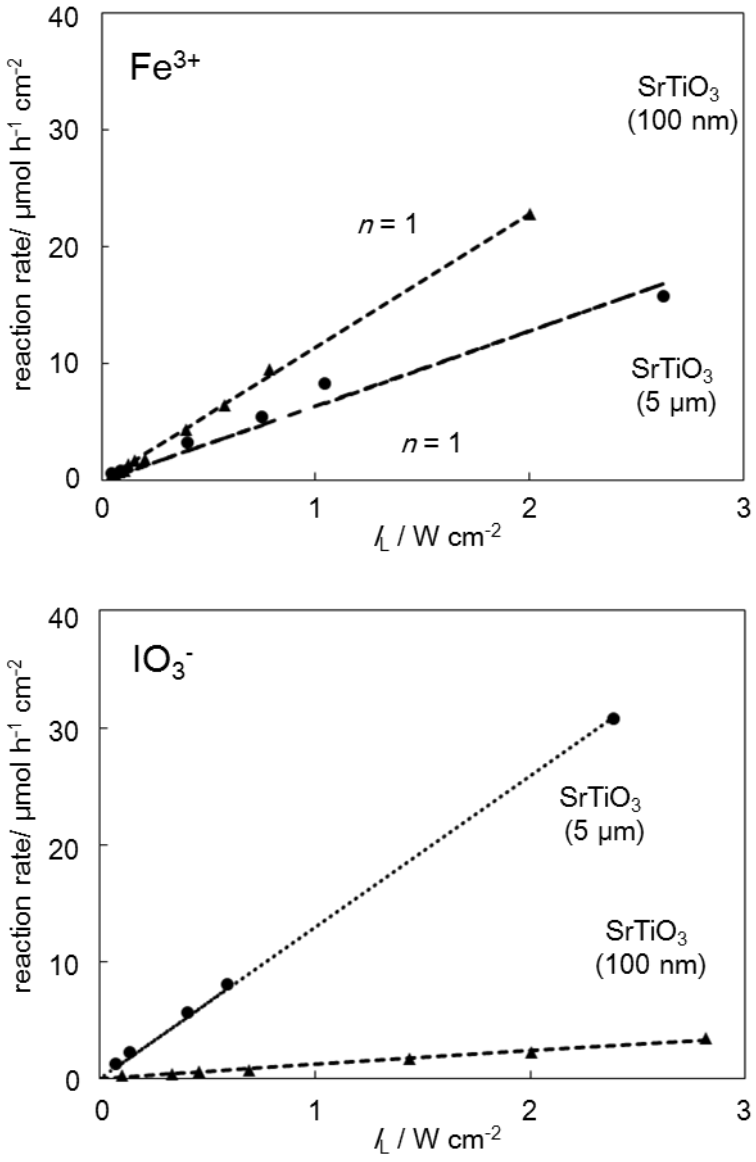

Fig.3-9 Light-intensity dependence of reaction rate of oxygen evolution using two type of $SrTiO_3$ samples in the presence of electron acceptor (IO_3^-, Fe^{3+})

3-6-3 Electron Acceptor Effect

On the **Table 1** shows the effect of electron acceptors for reaction rate and I_{thr} using IO_3^- and Fe^{3+} as an acceptor. Compared with SR and SA system for IO_3^- and Fe^{3+} system, I_{thr} and reaction rate became higher in Fe^{3+} system than IO_3^-. In the case of SR using as photocatalyst, the electron transfer (positive hole production) efficiency φ of Fe^{3+} system was thirteen times higher than that of IO_3^- system. This fact was indicated that the excited electron transfer to Fe^{3+} was faster than that to IO_3^-. It is suggested that the one-electron reduction of Fe^{3+} proceed faster than the reduction of IO_3^-.

In contrast, the difference of I_{thr} for Fe^{3+} and IO_3^- system using SR was indicated the relative value of the inverse of threshold intensity which defined as $\varphi\tau_1$ in Fe^{3+} system was much smaller than IO_3^- system. According to above analysis, it was suggested the φ in Fe^{3+} system was higher than that of IO_3^- system. Therefore, the higher I_{thr} of Fe^{3+} system than IO_3^- system was due to the lifetime of positive hole of TiO_2 is shorter than IO_3^-. When the reaction rate of reversed electron transfer process between positive hole and reductive product in Fe^{3+} system was faster than the IO_3^-, the lifetime of positive hole in $TiO_2(h^+)$, τ_1 become shorter, and then, the threshold become higher. Moreover, in the case of SA system also observed I_{thr} in Fe^{3+} system higher than IO_3^- system. It was suggested the reaction rate of reversed reaction was also affected to the light-intensity dependence and overall reaction rate.

In this kinetic analysis, the lifetime of positive hole was presumed from the inverse of the number of incident photon ($N_{incident}$) in one photocatalyst particle in one second which meant the interval of another photon incidence. $N_{incident}$ can be derived using planck constant (h), light speed(c) and the wavelength of irradiation light(λ) as shown below.

$$N_{incident}(/s) = I_L/(N_A hc/\lambda) \qquad (48)$$

According to the previous reports, it was generally discussed the lifetime of charge carrier become Pico second-order under laser excitation, and it was described the probability of recombination were increased in the multiple charge carrier existing in one photocatalyst particle [Ohtani 1998, Bacher 1999]. However, the presumed lifetime in this study were as micro second-order (**Table 3-2**) due to electron acceptor capturing the excited electron in the system, therefore the lifetime of hole can be prolonged. Furthermore, the excitation intensity of UV-LED is much lower than laser light source, thus, the higher order of recombination process can be neglected.

Table 3-1 Physical/structural properties of titania samples and kinetic parameters for photocatalytic oxygen evolution.

code	supplier[a]	product name	anatase[b] (%)	rutile[b] (%)	non-crystal[b] (%)	SSA[c] /$m^2 g^{-1}$	PPS[d] /nm	SPS[e] /μm	r (IO_3^-)[f]	r (Fe^{3+})[f]	I_{thr}[g] /W cm^{-2} (IO_3^-)	I_{thr}[g] /W cm^{-2} (Fe^{3+})
SA	IS	ST-01	79.9	0	20.1	344	8	5.9	6	2	0.16	0.98
SR	Tayca	MT-150A	0	81.9	18.1	114	14	—	4	44	0.15	0.36
LA	Fluka	—	93.3	3.3	3.4	9	172	0.6	2	7	—	—
LR	SDC	ST-G2	3.0	94.8	2.2	4	500	0.9	268	144	—	—
SR973	Tayca	MT-150A	0	91.2	8.8	22	83	—	37	31	0.028	0.019

[a]IS: Ishihara Sangyo and SDC: Showa Denko Ceramics. [b]Estimated by Rietveld analysis of XRD patterns of a sample mixed with nickel(II) oxide as an internal standard. [c]Specific surface area estimated from nitrogen adsorption. [d] Primary particle size estimated from peak width in XRD patterns using the Scherrer equation. [e]Secondary particle size measured using a laser-diffraction particle-size analyzer. [f]Rate of oxygen evolution in the light-intensity region in which the order is unity. [g]Threshold light intensity for change of order from 2 to 1 (See the text.)

Table 3-2 Kinetic and photon incident properties caliculated from I_{thr}

TiO_2	particle size	acceptor	I_{thr}/W cm^{-2} (second to first order)	I'_{thr}/W cm^{-2} (first to fourth order)	$N_{incidnet}$ (I_{thr})	time for another photon incidence (I_{thr})/μs	$N_{incidnet}$ (I'_{thr})	time for another photon incidence (I'_{thr}) /μs
ST-01	4.4	IO_3^-	0.17	2.5	4.9.E+04	21	7.0.E+05	1.4
MT-150A	13	IO_3^-	0.19	-	4.7.E+05	2.1	-	-
MT-150A(973K)	69	IO_3^-	0.025	-	1.9.E+06	0.53	-	-
MT-150A	13	Fe^{3+}	0.52	-	1.3.E+06	0.77	-	-
MT-150A(973K)	69	Fe^{3+}	0.019	-	1.3.E+06	0.75	-	-

3-7 Conclusions of Multielectron transfer Mechanism

It was discussed the light-intensity dependence based on the experimental data and kinetic analysis in photocatalytic oxygen evolution in the presence of electron acceptor to clarify the mechanism of multielectron transfer in heterogeneous photocatalysis. These results were suggested that irradiation light-intensity affected to the overall reaction rate and light-intensity dependence.

One of the significant finding was the higher-order dependence of oxygen evolution reaction. In that case of SR system, the second-to-first order dependence in the lower intensity region was observed, and also, the SA system was shown the second-order dependence, but surprisingly, the significant fourth-order dependence was observed in the higher intensity region. These higher order dependence observation is the first report in multielectron transfer process. Such the higher-order dependences in oxygen evolution reaction could be corresponded to the two-electron and four-electron transfer process. In general, it was discussed photocatalytic oxygen evolution have been considered proceeding by four-electron (positive-hole) transfer process ($2H_2O = O_2 + 4H^+ + 4e^-$:+1.23 V) based on SEP. However, the second-order dependence was observed in the low light intensity region due to the two-electron transfer process proceeding. In heterogeneous photocatalysis, the charge carriers are not guaranteed for redox reaction because the activity of electron transfer is not unity, therefore the number of carrier which can react with surface adsorbed substances are depending on the light-intensity. In the case of low intensity region, it was difficult to accumulate four positive-hole at the same time during the lifetime of one positive hole in one photocatalyst particle. In addition, the valance band top position is deep enough to drive the two-electron transfer process through hydrogen peroxide production ($2H_2O = H_2O_2 + 2H^+ + 2e^+$: + 1.76 V). Therefore, the two-electron reaction could proceed in the lower intensity condition which can be guaranteed two-electron (positive hole).

On the other hand, the fourth-order dependence observed in the higher intensity region can correspond to the four-electron transfer process due to the four positive-hole guaranteed under large number of photonabsorption condition. In this case, the standard electrode potential (SEP) of four-electron transfer process is lower than that of two-electron process as defined, therefore, the reaction mechanism of oxygen evolution is changed from two to four-electron process which can proceed lower energy based on SEP, i.e., thermodynamics. The mechanism of photocatalysis especially multielectron transfer process have been defined by SEPs, however, these finding suggest that the mechanism is affected not only the SEPs i.e. thermodynamics, but also the light intensity i.e. kinetics for the first time. These mechanism changing can not explain by ordinary kinetics which is the function of concentration of analogue value. The first to fourth-order, i.e., two to four-electron transfer process switching suggests the mechanism of multielectron transfer digitally controlled by the number of photon absorption. This is the first report of singularity in not only photocatalysis but also in chemical reaction.

On the other hand, a multielectron transfer process has also been reported for the photocatalytic organics oxidation accompanied by oxygen reduction in a bismuth tungstate-photocatalyzed reaction, in which higher-order LID was also observed [Hori 2017, Hori 2017b]. Hence, the correlation of thermodynamics and kinetics, which discussed above is suggested as the new fundamental aspect for heterogeneous photocatalysis.

The effect of a photocatalyst particle size and electron acceptor in photocatalytic oxygen evolution from water was indicated based on the kinetic analysis. The differences of reaction rate and threshold intensity (I_{thr}) in two electron transfer process are suggested that the efficiency of charge carrier production (φ), lifetime of positive hole (τ), and the photoabsorption efficiency of one-positive hole bearing TiO_2 (ψ') are depending on the effective particle-size and acceptor ion. These facts are indicated that in called "low activity" photocatalyst may be due to high I_{thr} to lead low reaction-rate affected high-order dependence under ordinary light source (e.g. mercury lamp, xenon lamp) intensity. Therefore, the high-intensity irradiation which is higher than I_{thr} and guarantee the multiple charge carrier production may improve the photocatalytic activity.

Above mentioned some findings, which are the correlation of thermodynamics and kinetics in photocatalytic multielectron transfer process, and kinetic analysis of the effect of acceptor ion and particle size in overall reaction rate and light intensity dependence are the significant issue in photochemistry and the novel concept for photocatalysis designing.

3-8 Reference

[Amano 2013] Amano, F., Ishinaga, E., Yamakata, A., Effect of Particle Size on the Photocatalytic Activity of WO_3 Particles for Water Oxidation, *J. Phys. Chem. C*, **117**, 22584−22590 (2013).

[Bacher 1999] Bacher, G., Weigand, R., Seufert, J., Kulakovskii, V. D., Gippius, N. A., Forchel, A., Biexciton versus Exciton Lifetime in a Single Semiconductor Quantum Dot, *Phys. Rev. Lett.*, **83**, 4417-4420 (1999).

[Bamwenda 2001] Bamwenda, G. R., Uesigi, T., Abe, Y., Sayama, K., Arakawa, H., The photocatalytic oxidation of water to O_2 over pure CeO_2, WO_3, and TiO_2 using Fe^{3+} and Ce^{4+} as electron acceptors, *Appl. Catal. A: General*, **205**, 117–128, (2001).

[Bard 1985] Bard, A. J.; Parsons, R.; Jordan, J., Standard Potentials in Aqueous Solution, *Marcel Dekker,* New York and Basel (1985).

[Fujihara 1998] Fujihara, K., Ohno, T., Matsumura, M., Splitting of water by electrochemical combination of two photocatalytic reactions on TiO2 particles. *J. Chem. Soc., Faraday Trans.*, **94**, 3705-3709 (1998).

[Fujihara 2000] Fujihara, K., Izumi, S., Ohno, T., Matsumura, M., Time-resolved photoluminescence of particulate TiO_2 photocatalysts suspended in aqueous solutions. *J. Photochem. Photobiol. A: Chem.*, **132**, 99-104 (2000).

[Fleischauer 1972] Fleischauer, P. D., Alan Kan, H. K., Quantum Yields of Silver Ion Reduction on Titanium Dioxide and Zinc Oxide Single Crystals, *J. Am. Chem. Soc.*, **94** 283-285 (1972).

[Hong 2009] Hong, S. J., Jun, H., Borse, P. H., Lee, J. S., Size effects of WO_3 nanocrystals for photooxidation of water in particulate suspension and photoelectrochemical film systems, *International Journal of hydrogen energy*, **34** 3234-3242 (2009).

[Hori 2017] Hori, H., Takashima, M., Takase, M., Ohtani, B., Pristine Bismuth-tungstate Photocatalyst Particles Driving Organics Decomposition through Multielectron Reduction of Oxygen. *Chem. Lett.*, **46**, 1376-1378 (2017).

[Hori 2017b] Hori, H., Takashima, M., Takase, M., Kitamura, M., Amano, F., Ohtani, B., Multielectron reduction of molecular oxygen in photocatalytic decomposition of organic

compounds by bismuth tungstate particles without cocatalyst loading. *Catal. Today*, DOI: 10.1016/j.cattod.2017.08.045 (2017).

[Prieto 2009] Prieto-Mahaney, O.-O., Murakami, N., Abe, R., Ohtani, B. Correlation between Photocatalytic Activities and Structural and Physical Properties of Titanium(IV) Oxide Powders. *Chem. Lett.*, **38**, 238-239 (2009).

[Maeda 2014] Maeda, K. Effects of the Physicochemical Properties of Rutile Titania Powder on Photocatalytic Water Oxidation. ACS Catal. 4, 1632-1636 (2014).

[Mikhaylov 2012] Mikhaylov, R.V., Lisachenko, A.A., Titov, V. V., Investigation of Photostimulated Oxygen Isotope Exchange on TiO_2 Degussa P25 Surface upon UV−Vis Irradiation. *J. Phys. Chem. C* **116**, 23332-23341 (2012).

[Murakami 2007] Murakami, S., Kominami, H., Kera, Y., Ikeda, S., Noguchi, H., Uosaki, K., Ohtani, B., Evaluation of electron–hole recombination properties of titanium(IV) oxide particles with high photocatalytic activity, *Res. Chem. Intermed.*, **33** 285–296 (2007).

[Ohno 1997] Ohno, T., Haga, D., Fujihara, K., Kaizaki, K., Matsumura, M., Unique Effects of Iron(III) Ions on Photocatalytic and Photoelectrochemical Properties of Titanium Dioxide, *J. Phys. Chem. B*, **101**, 6415-6419 (1997).

[Ohno 2001] Ohno, T., Sarukawa, K., Matsumura, M. Photocatalytic Activities of Pure Rutile Particles Isolated from TiO2 Powder by Dissolving the Anatase Component in HF Solution. *J. Phys. Chem. B*, **105**, 2417-2420 (2001).

[Ohtani 1998] Ohtani, B., Bowman, R.M., Colombo, Jr, D.P., Kominami,H., Noguchi, H., Uosaki, K., Femtosecond Diffuse Reflectance Spectroscopy of Aqueous Titanium(IV) Oxide Suspension: Correlation of Electron-Hole Recombination Kinetics with Photocatalytic Activity, *Chem. Lett.*, **7**, 579-580 (1998).

[Ohtani 2010] Ohtani, B., Prieto-Mahaney, O.-O., Amano, F., Murakami, N., Abe, R. What Are Titania Photocatalysts?—An Exploratory Correlation of Photocatalytic Activity with Structural and Physical Properties. *J. Adv. Oxidat. Tech.*, **13**, 247-261 (2010).

[Sato 1984] Sato, S., Kadowaki, T., Yamaguti, K., Photocatalytic Oxygen Isotopic Exchange between Oxygen Molecule and the Lattice Oxygen of TiO_2 Prepared from Titanium Hydroxide. *J. Phys. Chem.* **88**, 2930-2931 (1984).

[Sato 1987] Sato, S., Kadowaki, T., Photocatalytic Activities of Metal Oxide Semiconductors for Oxygen Isotope Exchange and Oxidation Reactions. *Journal of Catalysis* **106**, 295-300 (1987).

Chapter 4

Discussion on the Mechanism of Co-catalyst in Heterogeneous Photocatalysis

4-1 Introduction

As already described in **Chapter 1**, there are many reports about the improvement of reaction efficiency by co-catalyst deposited on the photocatalyst surface. It was discussed that the mechanism of photocatalytic reaction efficiency improvement by co-catalyst was mainly due to the enhanced charge-separation efficiency and/or inhibition of recombination between excited electron-positive hole. Therefore, the co-catalyst deposition is necessary used and disucussed especially in artificial photosynthesis, water splitting and/or carbon dioxide reduction to improve the efficiency for achievement of commercialization. However, the role of co-catalyst in photocatalysis, especially in multielectron transfer process is not clarified yet. In general, the effect of co-catalyst was usually discussed by the difference of reaction rate between before and after depositon [Kato 2001, Ma 2009, Sasaki 2008, Yang 2013, Hisatomi 2015]. On the other hand, some researchers were discussed the role of co-catalyst by the transient absorption analysis using pump-probe method with laser irradiation and suggested the lifetime of charge carrier increasing due to the charge migration [Zhang 2014, Li 2006, Barosso 2014]. Although, there was no report about the qualitative analysis of the correlation of photocatalytic activity and co-catalyst effect though the essential role of co-catalyst in photocatalysis is still unknown.

In **chapter 3**, the kinetic analysis of photocatalytic oxygen evolution was discussed about the effect of particle-size and electron acceptor based on the kinetic equation of two-electron transfer process according to the second to first-order light-intensity dependence observed in the UV-LED intensity range. In that case, it is available for quantitative analysis of the influence of these effects using several kinetic parameters.

In this chapter, the effect of co-catalyst in photocatalytic oxygen evolution was discussed by kinetic analysis for clarification of the role of co-catalyst. Co-catalysts were deposited on the small rutile TiO_2, MT-150A in which observed the second to first-order dependence under UV-LED irradiation condition. In this study, iridium oxide (IrO_2), manganese oxide (MnO_2), and cobalt phosphate (Co-Pi) were used as a co-catalyst. The analysis of light-intensity dependence of reaction rate under suspended co-catalyst loaded MT-150A were given some information the difference of threshold intensity and reaction rate as presented below.

4-2 Light-intensity Dependence Analysis in Co-catalyst Loaded TiO_2

4-2-1 0.1wt% MnO_2, IrO_2 and Co-Pi Loaded on Rutile Samples

In this study, all co-catalysts were deposited by photodeposition method which were already described the detail in **chapter 2**. The deposited co-catalyst were chosen as iridium oxide (IrO_2), manganese oxide (MnO_2) and cobalt phosphate (Co-Pi) which were well known as the co-catalyst in photocatalysis especially water oxidation (splitting). **Fig.4-1** showed the light-intensity dependences of photocatalytic oxygen evolution reaction in IO_3^- as an acceptor and its double-logarithm plot. The plots of bare MT-150A system were used as the same of **chapter 3**.

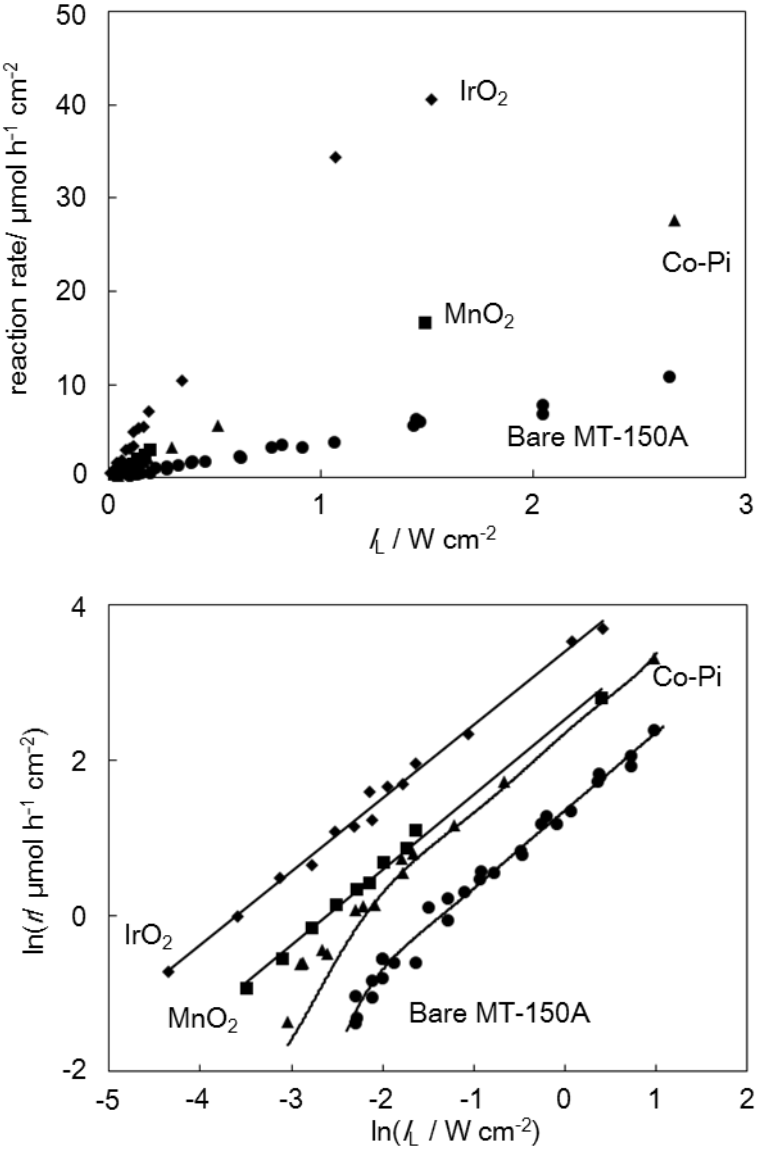

Fig. 4-1 light-intensity dependence of reaction rate and double-logarithm plot for each 0.1 wt% co-catalyst loaded titania samples in the presence of IO_3^- as an electron

According to the **Fig.4-1**, the reaction rate were enhanced for all co-catalyst loaded sample than the bare TiO_2, however, the light-intensity dependency was clearly different between IrO_2, MnO_2 and Co-Pi loaded sample. In the case of Co-Pi loaded sample, overall reaction rate was increased from bare TiO_2, although, the tendency of light-intensity dependence was almost same, i.e. the second to first-order dependence didn't change after deposition. On the other hand, the higher-order dependence was not observed in IrO_2 or MnO_2 loaded sample. The overall reaction rate of IrO_2 was higher than MnO_2 loaded sample, though the dependency was observed only first-order. In addition, it was considered the light-intensity dependence of the mixture sample of TiO_2 and co-catalyst material as the control experiment. The non-deposited sample was prepared by mixing with MT-150A and 0.1 wt% amount of Manganese oxide (IV) (MnO_2: Wako pure chemical

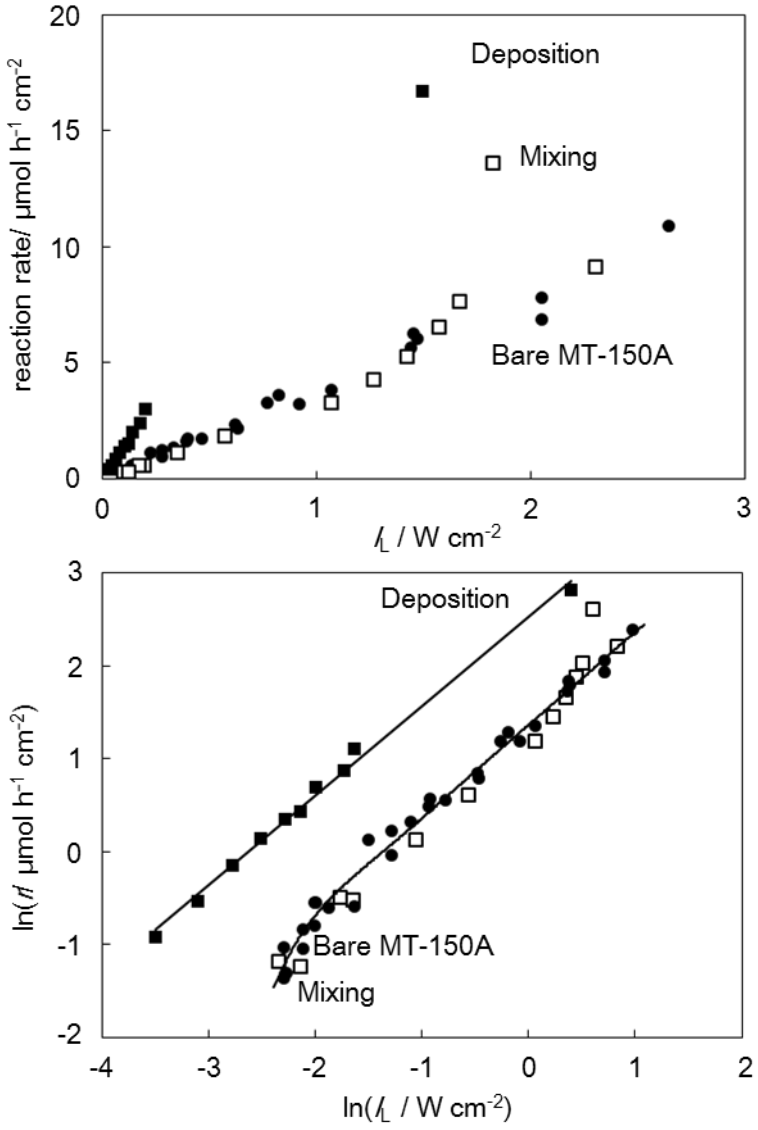

Fig. 4-2 light-intensity dependence of reaction rate and double-logarithm plot for 0.1 wt% MnO_2 deposited and mixed titania samples in the presence of IO_3^- as an electron acceptor.

industry) using mortal agate for 5 min. However, the reaction rate and threshold intensity of MnO_2-MT-150A observed as the almost same as the bare MT-150A system. This fact suggested that non-deposited MnO_2 was not affected to photocatalytic reaction efficiency (**Fig. 4-2**). The particle-size and/or dispersibility of co-catalyst were different for photodeposition and mixing method, hence there is no influence for overall reaction rate and dependency. Therefore, the particle-size of co-catalyst which is loaded on the photocatalyst surface can affect to the photocatalytic activity.

These different light-intensity dependences observation in multielectron reaction depending on the kinds of loaded co-catalyst are the first time report in this research field, and this fact provides the new perspective about co-catalyst. According to these different dependencies, it suggest that the mechanism of improvement of reaction efficiency differed in each co-catalyst, and kinetic analysis of these dependencies were described in **section 4-3**.

4-2-2 Influence for the Loading Amount of Co-catalyst

In the heterogeneous photocatalysis, it has been well considered the amount of co-catalyst is one of the important factor. If overage amount of co-catalyst loaded on the photcatalyst than optimum amount, photoabsorption might be reduced due to coverage the surface of photocatalyst, and decreased photocatalytic activity. Therefore, the kinetic analysis for the effect of loaded amount of effect is one of the interesting factor in photocatalytic multielectron reaction.

In this study, it was discussed the amount of loading co-catalyst affecting to the light-intensity dependence using MnO_2 loaded on MT-150A. **Fig. 4-3** showed the light intensity dependence of reaction rate using different amount of MnO_2 loaded MT-150A in the presence of IO_3^- as an acceptor. As already shown in **Fig. 4-1**, the first-order dependence was observed in 0.1 wt% MnO_2 loaded MT-150A sample. However, 0.5 wt% loaded sample, the threshold of second-to-first-order dependence (I_{thr}) was appeared in the middle range of light intensity. The overall reaction rate was lower than 0.1 wt% loaded sample, but higher than the bare sample. The reason of appearance I_{thr} in 0.5wt% MnO_2 loaded MT-150A was suggested due to some kinetic parameters changing. According to the influence of amount of MnO_2, the kinetic analysis was discussed as following **section 4-3**.

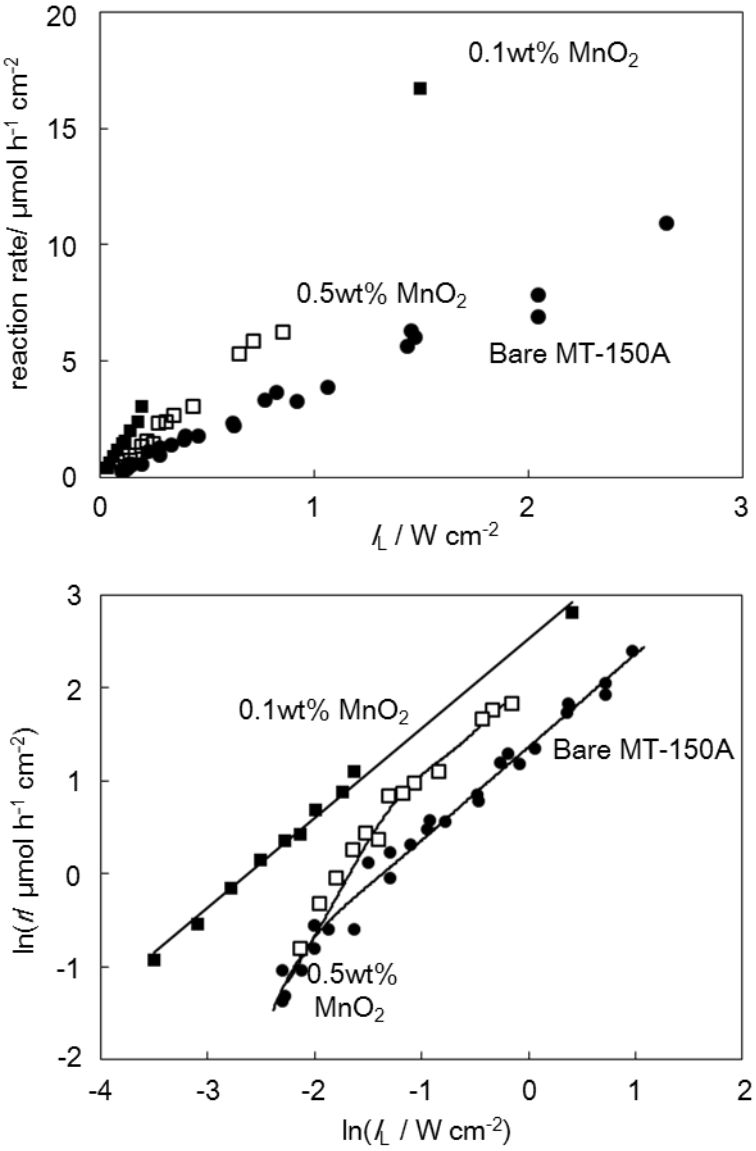

Fig. 4-3 Double-logarithm plot of light-intensity dependence of reaction rate for different amount MnO_2 loaded titania samples in the presence of IO_3^- as an electron acceptor.

4-3 Kinetic Analysis of Co-catalyst Loading Effect for Multielectron Transfer

As already described in above section, it was analyzed the light intensity dependence of oxygen evolution reaction rate in co-catalyst loading on the MT-150A system. In **chapter 3**, the kinetic analysis was discussed according to the two-electron transfer reaction model, and its derived kinetic equations. In that case, it was considered the influence of particle-size and electron acceptors affecting to the overall reaction rate and light intensity dependence quantitatively using kinetic parameters. According to the analysis, it was also discussed the influence of co-catalyst effect in photocatalytic oxygen evolution.

As already shown, the influence of co-catalyst affected to the overall reaction rate and threshold intensity (I_{thr}). The reaction rate of first-order dependence corresponding to the efficiency of positive-hole production (φ) was increasing for each co-catalyst loaded sample than bare MT-150A. In the first-order dependence light intensity region, the lifetime of positive hole (τ_2) was not included and depending in the Eq. (30), it was not sure about the influence for τ_2, although φ was improved at least by each co-catalyst deposition (**Table 4-1**).

On the other hand, the difference of I_{thr} for each samples, the relative value of MnO_2 and IrO_2 were quite higher (> 8 times) than the bare and Co-Pi loaded sample because there were no observation of second-order dependence in the measurement light intensity range. The particle-size which calculated from specific surface area were almost same for each samples, hence photoabsorption efficiency of one positive hole-bearing TiO_2 ($TiO_2(h^+)$)(ψ_2) might be not influenced by the physical property of TiO_2. In the case of Co-pi system, φ was increased according to the reaction rate increasing, however, I_{thr} was not so different from bare sample. Thus, τ_1 might be decreased and increased of φ due to Co-Pi deposition, respectively. Therefore, it was suggested the deposited Co-pi might not contribute to positive hole pooling. On the other hand, MnO_2 and IrO_2 deposition sample, I_{thr} was not observed (or lower than the detection limited intensity). Therefore, it was suggested that τ_1 were not decreased by MnO_2 and IrO_2 deposition due to positive hole pooling. These facts are indicated that the role of co-catalyst which improve the photocatalysis reaction efficiency is different according to the kind of loading co-catalyst.

In the case of the analysis of amount of co-catalyst loading in **Fig. 4-3**, the system of 0.5 wt% MnO_2 loading sample was observed lower reaction rate and higher I_{thr} than 0.1 wt% loading sample. It was suggested that the overage amount of MnO_2 loading induces the reducing of ψ_2 due to coverage of TiO_2 surface and/or decreasing of τ_1 than 0.1 wt% sample. In this case, the I_{thr} of 0.5 wt% is higher than the bare MT-150A. Thus, it suggests that ψ_2 is mainly reduced according to above kinetic analysis. The possible reason for those light-intensity dependence is the influence of the difference of particle-size and/or the number of co-catalyst deposited on the surface of TiO_2 according to the kinds of co-catalyst. When the number co-catalyst (m) deposited on the surface, the probability of multiple hole accumulation in one co-catalyst particle can

decrease, therefore, the effective particle-size (guaranteed the multiple photon absorption) can be affected as 1/*m*. Therefore, the probability of accumulation of positive hole was reduced due to the positive hole dispersion and the ψ_2 might be decreased. It is suggested the number of co-catalyst deposition on the surface is one of the important factor for reaction rate. In addition, the photodeposition can preferably occur at larger particle than smaller based on the particle size distribution.

Table 4-1 Kinetic parameters co-catalyst loading titania samples for photocatalytic oxygen evolution

Co-catalyst	photocatalyst	loaded amount(wt%)	relative rate (IO_3^-)	I_{thr} (IO_3^-) /W cm^{-2}
-	MT-150A	-	1	0.16
Co-Pi	MT-150A	0.1	2.7	0.12
MnO_2	MT-150A	0.1	3.6	< 1
MnO_2	MT-150A	0.1 (mixture)	0.9	< 1
MnO_2	MT-150A	0.5	2.0	0.27
IrO_2	MT-150A	0.1	7.6	< 0.01

4-4 Co-catalyst Loading Small Anatase TiO_2

As already showed in above, it was observed that the reaction order of light intensity was changed from second to first, and fourth-order according to the light intensity using the small anatase TiO_2 (ST-01) in the presence of IO_3^- ion as an acceptor. In that case, it was suggested that the number of accumulated positive hole in one photocatalyst particle was corresponding to the multielectron reaction mechanism, hence the co-catalyst deposition may affected the reaction rate and/or light-intensity dependence. Therefore, it was discussed about the co-catalyst deposition for ST-01 and the analysis of light-intensity dependence of reaction rate.

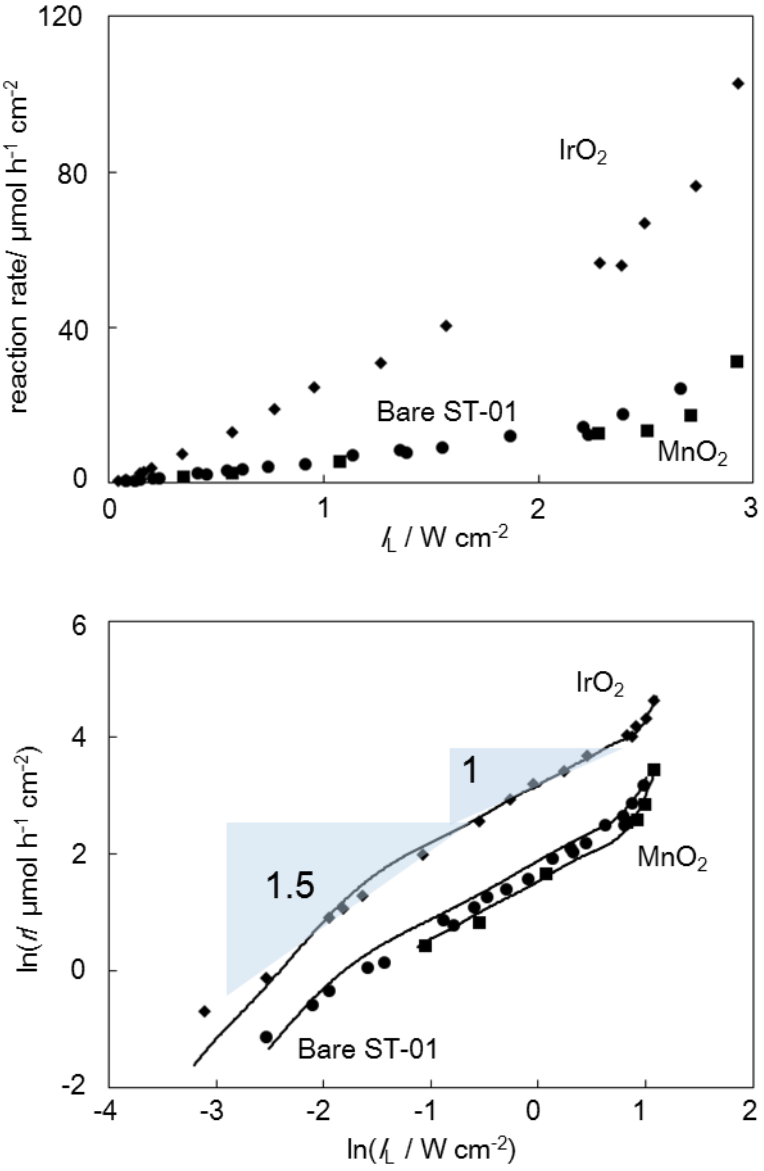

Fig. 4-4 Double-logarithm plot of light-intensity dependence of reaction rate for Co-catalyst loaded ST-01 in the presence of IO_3^- as an electron acceptor.

Fig.4-4 indicated the reaction rate of oxygen evolution in the presence of IO_3^- for each co-catalyst loading samples. IrO_2 loaded sample was 5 times higher rate than bare ST-01 observed, however the light-intensity dependence was shown almost same tendency. The number of plots were not enough in MnO_2 loaded sample, but the dependence was almost same and the reaction rate was not improved after deposition. In the case of MT-150A system, light intensity dependences were quite different according to the kinds of co-catalyst. It was suggested that the different influences of co-catalyst in anatase and rutile sample were due to the correlation of co-catalyst and photocatalyst, and/or a particle-size of loading co-catalyst. The particle-size of MT-150A is three times higher than ST-01, therefore, particle-size and their disparsibility might be different based on their physical property. Another possible reason on the dependencies in ST-01 system due to the influence of particle-size distribution. When ST-01 is composed by the mixture of large and small size particle, the probability of photodeposition become preferably higher in large particle than small one. The almost 1.5 th-order of double logarithm plot in the lower intensity region might be due to the mixture of second-order of small particle and first-order of large particle. Therefore the I_{thr} is almost same comparing with IrO_2 and bare ST-01 because the I_{thr} is controlled by the effective particle size of smaller particles.

4-5 Influence of Co-catalyst in Kinetics of Multielectron Transfer Process

As shown above section, it was discussed about the light intensity dependence of oxygen evolution reaction using co-catalyst loaded TiO_2 samples to clarify the role of co-catalysis. The kinetic analysis using the equation derived from the two-electron transfer model using in **chapter 3** was suggested some significant findings. According to the analysis of light-intensity dependence using co-catalyst loading samples, it was observed the different dependence for each co-catalyst system and indicated that the role of MnO_2 and IrO_2 was different compared with Co-Pi as a co-catalyst. In the case of small rutile TiO_2 system, these different tendencies based on the reaction rate and light-intensity dependence were suggested due to the efficiency of positive hole production depending on the kind of co-catalyst, therefore, the efficiency was affected the possibility of multi-positive hole bearing in one photocatalyst. On the other hand in small anatase TiO_2 system, it was suggested the number of deposited co-catalyst on one photocatalyst particle as the important factor for the effective particle size. In addition, the method of co-catalyst deposition may be also affect to the kinetic parameters.

As shown above, these significant findings based on the kinetic analysis may be the first report to estimate the role of co-catalyst by the kinetic analysis and it can be potentially applied for the new novel method for designing photocatalysis.

4-6 References

[Barosso 2014] Barroso, M., Cowan, A. J., Pendlebyry, S. R., Gratzel, M., Klug, D. R., Durrant, J.R., The Role of Cobalt Phosphate in Enhancing the Photocatalytic Activity of α-Fe_2O_3 toward Water Oxidation, *J. Am. Chem. Soc.*, **133**, 14868−14871 (2011).

[Hisatomi 2015] Hisatomi, T., Takanabe, K., Domen, K., Photocatalytic Water-Splitting Reaction from Catalytic and Kinetic Perspectives, *Catal. Lett.*, **145**, 95–108 (2015).

[Kato 2001] Kato, H., Kudo, A., Water Splitting into H_2 and O_2 on Alkali Tantalate Photocatalysts $ATaO_3$ (A = Li, Na, and K), *J. Phys. Chem. B*, **105**, 4285-4292 (2001).

[Li 2006] Li, H., Bian, Z., Zhu, J., Huo, Y., Li, H., Lu, Y., Mesoporous Au/TiO_2 Nanocomposites with Enhanced Photocatalytic Activity, *J. Am. Chem. Soc.*, **129**, 4538−4539 (2007).

[Ma 2009] Ma, B., Wen, F., Jiang, H., Yang, J., Ying, P., Li, C., The Synergistic Effects of Two Co-catalysts on Zn_2GeO_4 on Photocatalytic Water Splitting, *Catal. Lett.*, **134**, 78–86 (2010).

[Maeda 2010] Maeda, K., Domen, K., Photocatalytic Water Splitting: Recent Progress and Future Challenges, *J. Phys. Chem. Lett.*, **1**, 2655–2661 (2010)

[Sasaki 2008] Sasaki, Y., Iwase, A., Kato, H., Kudo, A., The effect of co-catalyst for Z-scheme photocatalysis systems with an Fe^{3+}/Fe^{2+} electron mediator on overall water splitting under visible light irradiation, *Journal of Catalysis*, **259**, 133–137 (2008).

[Yang 2013] Yang, J., Wang, D., Han, H., Li, C., Roles of Cocatalysts in Photocatalysis and Photoelectrocatalysis, *Account of Chemical Research*, **46**, 1900-1909 (2013)

[Zhang 2014] Zhang, F., Yamakata, A., Maeda, K., Moriya, Y., Takata, T., Kubota, J., Teshima, K., Oishi, S., Domen, K., Cobalt-Modified Porous Single-Crystalline $LaTiO_2N$ for Highly Efficient Water Oxidation under Visible Light, *J. Am. Chem. Soc.*, **134**, 8348−8351 (2012).

Chapter 5

5-1 General Conclusions

Light-intensity dependence of the rate of photocatalytic oxygen evolution from the suspensions of various titania powders in the presence of electron donors was studied using UV-LEDs emitting light of intensity one or two orders higher than ordinary continuous light sources. Bimodal dependence, second and first order in the relatively lower and middle intensity ranges, respectively, commonly observed for small anatase and rutile titania photocatalysts suggested that two-electron oxidation to yield hydrogen peroxide as a labile reaction intermediate proceeds under the present UV-LED irradiation. A kinetic model derived assuming photocatalyst particles are activated only when two positive holes are accumulated could reproduce this bimodal dependence; at the lower intensity range, probability of creation of two positive-hole bearing particles is increased in proportion to the square of light intensity to show the second-order dependence, while at the middle intensity range, creation of two positive-hole bearing particles is guaranteed to show the first-order dependence, though two-electron oxidation still proceeds in this range. The linear (first order) dependence of large anatase and rutile titania photocatalysts in the whole intensity range can be interpreted as that for those large particles the creation of two positive-hole bearing particles is guaranteed under the intense UV-LED irradiation since the probability of absorption of second photons by one positive-hole bearing particles, though the possibility of four-electron oxidation cannot be ruled. Thus, it is indicated that titania photocatalysts liberate oxygen via two electron-oxidation process for the first time based on the kinetic analysis. Since oxidation ability of titania is high, i.e., VB-top energy is sufficiently more anodic than the SEP for two electron-oxidation process and once liberated hydrogen peroxide undergoes rapid further oxidation to oxygen. The frequently reported low or negligible photocatalytic activity of anatase titania samples under conventional continuous photoirradiation might be owing to excessively low light intensity at which the order of light-intensity dependence is two, while rutile titania tends to have larger particle size to show first-order dependence even in the lower intensity range. In the conventional studies on photocatalysis, effect of particle size of photocatalysts has been explained by the difference in specific surface area which regulates the amount of surface-adsorbed reaction substrates. However, the above-mentioned results suggest that particle size influences the probability of multiphoton absorption in each particle and size of a part of particles in which photogenerated charge carriers can participate, i.e., effective particle size for multiphoton absorption, as a novel concept, is important.

When small anatase titania was used, forth-order light-intensity dependence was observed in addition to the bimodal dependence at the highest intensity range and this unconventional high-

order dependence is accounted for by four-electron oxidation of water, i.e., four electron-bearing particles could be created at the highest intensity region. Different from the change in the order from to two to one in the middle intensity range in which the order was changed smoothly, the order seemed to suddenly changed from one to four, i.e., the curve of light-intensity dependence exhibited "singularity". As far as the author knows, this is the first example of singularity in chemistry. The singularity is explained by the change in the number of transferred electrons from two to four. Such a change in the reaction path, observed presumably for the first time, means the reaction kinetics is regulated digitally by the number of transferred electrons.

Thus, the light intensity-dependence analysis using high-intensity UV-LED enabled the elucidation of the number of transferred electrons as the most significant parameter for multielectron processes. This methodology could be successfully applied to the studies on the effect of co-catalyst loadings. The results of light intensity-dependence analysis indicated that the mechanism of acceleration of oxygen evolution by co-catalyst loading is not straightforward; enhancement of creation of a trapped positive hole, extension of its lifetime and change in effective particle size of base titania particles may be included depending on the kinds of co-catalysts and their amount (density) on the surface of titania photocatalysts.

5-2 Future Aspects

Several novel insights have been obtained in this study.

(1) Significance of light intensity-dependence analysis: Kinetic studies for clarification of reaction mechanism has been recognized to be only supportive but not decisive, because assumptions are necessary for derivation of a kinetic model which reproduces the experimental results and it is impossible to exclude the other possible kinetic models. However, it was revealed in this study that at least for elucidation of the number of transferred electrons in multielectron processes, the kinetic analysis based on light-intensity dependence may be the sole possible method at present. Product analytical study, e.g., detection of labile intermediates such as hydrogen peroxide, as the two electron-process product, cannot give any information on the mechanism, since a one electron-process product can be further oxidized into hydrogen peroxide and there seems no reason for hydrogen peroxide to remain in the reaction mixture. Furthermore, introduction of a parameter, number of electrons accumulated in each photocatalyst particle, to a kinetic model enables to explain digitally regulated kinetics.

(2) Singularity—digitally regulated kinetics: In the conventional chemical-reaction kinetics, every functions vary continuously and smoothly without any discontinuous change. One of the possible reasons for this continuousness is that all the parameters included in a kinetic model are

of analogue value. However, the kinetic model used in this study is derived using a parameter, number of accumulated electrons, of digital value, i.e., no reaction is presumed if the number is one while two-electron oxidation proceeds when the number becomes two. Thus taking into consideration the number of absorbed photons and/or accumulated charge carriers in each photocatalyst particle, which has not been employed in the conventional studies on photocatalysis, might lead to this novel insight.

(3) Particle-size effect: In the previous studies on heterogeneous photocatalysis, photocatalyst particle size has been related to the size (area) of surface where reaction substrates are adsorbed and reacted with photoexcited electrons and positive holes. The results in this study, however, suggested that particle size could be defined the size of particles working as one unit of reaction, i.e., photoexcited electrons or positive holes created within the part of "effective particle size" collaborate to drive multielectron processes. The light intensity-dependence analysis is useful for elucidation of this effective particle size, and loosely aggregated can be counted as a particles and the effective particle size can be smaller than the apparent particle size for large particles. This novel concept, effective particle size can be applied for design of highly efficient photocatalyst.

(4) Effect of photon density on the overall rate: In the intensity range where the order of light-intensity dependence is higher than unity, the rate can be increased only by focusing the light beam without changing total light intensity. For example, in the case where the order is two, the rate is doubled when the light beam is focused to irradiate the halved area with doubled (area-unit) intensity. This should be noted in the reactor design for practical applications. On the contrary, reason for negligible activity of a given photocatalyst under ordinary continuous light irradiation might be such lower photon density in the irradiated area, but not the intrinsic photocatalytic activity.

(5) Challenge in oxygen evolution without using electron acceptors: Artificial photosynthesis aims at producing fuels in the reduction process as a counter reaction of oxygen evolution. The results of present results liberating oxygen using electron acceptors, but not water or carbon dioxide, tells that the accumulation of positive holes in each particle to drive oxygen evolution is less efficient even in the presence of electron acceptors, and it is easily expected that the efficiency of reaction in the absence of electron acceptors is very low or negligible. Alternatively, we should clarify the mechanism which enables the accumulation in the reported successful results.

Acknowledgments

First of all, I would like to appreciate Prof. Bunsho Ohtani, who provide me this precious study opportunity as a Ph.D. student in his laboratory and also great assistance in developing this experiment and doctoral thesis.

I also appreciate to Prof. Katsuaki Konishi (Hokkaido Univ.), Prof. Vasudevan Pillai, Biju (Hokkaido Univ.), and Prof. Mai Takase (Muroran Inst. Tech.) for helpful suggestions as the vice examiners.

I am very grateful to Prof. Mai Takashima and Mr. Shun Yoshihara to valuable cooperation for my experiments and making my thesis. And also, I would like to give great thanks for all Ohtani's lab. members in laboratory life.

Finally, I want to give a lot of thanks for my family and friends who always support my student life.

March 2018

Shugo Takeuchi